Influence of a Predecessor Rain Event on the Track of Tropical Cyclone Isaac (2012)

THOMAS J. GALARNEAU JR.

National Center for Atmospheric Research,* Boulder, Colorado

ABSTRACT

Analysis of a predecessor rain event (PRE) over the Straits of Florida ahead of Tropical Cyclone (TC) Isaac on 25 August 2012 is presented. This PRE is unique compared to previously documented PREs in midlatitudes because it occurred over the oceanic subtropics and impacted the track of an approaching TC. The Isaac PRE developed in conjunction with a tropical moisture plume with precipitable water values over 60 mm that intersected a region of mid- and upper-level frontogenesis and warm air advection on the southeast flank of an upper-level trough. The PRE occurred in an environment with more abundant tropical moisture and weaker synoptic-scale forcing for ascent compared to the environments in which midlatitude PREs developed.

The Isaac PRE contributed to the fracture of the upper-level trough through negative potential vorticity advection by convectively driven divergent outflow. Fracture of the upper-level trough and midlevel cyclonic vorticity amplification associated with the PRE acted to steer Isaac south of Florida into the Gulf of Mexico. Forecasts from the National Centers for Environmental Prediction–Global Forecast System (NCEP–GFS) initialized at 0000 UTC 21–24 August 2012 failed to predict the PRE and as a result recurved TC Isaac over Florida and the eastern Gulf of Mexico rather than continued Isaac on a northwest course toward southeast Louisiana. Vorticity inversion and detailed diagnosis of the NCEP–GFS TC track forecast initialized at 0000 UTC 22 August is also presented to assess the relationship between the PRE and TC Isaac's track.

1. Introduction

Predecessor rain events (PREs) are coherent high-impact mesoscale precipitation systems that occur ahead of tropical cyclones (TCs). PREs occur as tropical moisture is transported ahead of a TC and is lifted along a low-level frontogenetical baroclinic zone in the equatorward entrance region of an upper-level jet streak (e.g., Cote 2007; Galarneau et al. 2010; Moore et al. 2013; Bosart and Carr 1978; Byun and Lee 2012). The synoptic-scale forcing for ascent and deep tropical moisture transported from the TC comprises the ingredients for heavy rainfall (Doswell et al. 1996), and sets the stage for the development of heavy-rain-producing mesoscale precipitation systems (e.g., Meng and Zhang 2012).

Compositing studies of PREs by Cote (2007) and Galarneau et al. (2010) show that they occur over the continental United States (CONUS) ~1000 km ahead of TCs, with nearly one-third of all TCs over the western North Atlantic during 1995–2008 producing at least one PRE. Case studies of PREs associated with TC Erin (2007) by Galarneau et al. (2010) and Schumacher et al. (2011), TC Ike (2008) by Bosart et al. (2012), and TC Rita (2005) by Moore et al. (2013) show that PREs develop in a synoptic-scale flow pattern that resembles the "frontal"-type flash flood scenario identified by Maddox et al. (1979).

Building on previous work by Cote (2007) and Galarneau et al. (2010), Moore et al. (2013) identified three distinct synoptic-scale weather patterns in which PREs occur in their compositing study of PREs over the CONUS east of the Rockies during 1988–2010. The three synoptic patterns identified are "jet in ridge" (JR), "southwesterly jet" (SJ), and "downstream confluence" [DC; see Fig. 20 in Moore et al. (2013)]. These composite categories have many of the same characteristics identified by Galarneau et al. (2010), primarily that PREs develop as moist air in the TC's circulation is transported poleward ahead of the

TC and forced to ascend near a low-level frontogenetical baroclinic zone beneath the equatorward jet entrance region of an upper-level jet streak.

Moore et al. (2013) also discussed the role of the TC in PRE development for the three synoptic patterns identified. For TCs that (i) provide anomalously high water vapor transported to the PRE region by strong low-level southerly flow and (ii) strengthen and anchor the upper-level jet streak through combined diabatically driven divergent outflow from the TC and developing PRE, their role is considered *direct*. The SJ and DC synoptic patterns fall into this category. In addition to providing high water vapor, these TCs have a dynamical impact on the developing PRE. Strengthening and anchoring of the upper-level jet by the TC and developing PRE can also facilitate the development of subsequent PREs (Bosart et al. 2012) and atmospheric rivers (Cordeira et al. 2013). For TCs that provide anomalously high water vapor only, their role is considered *indirect*. The JR synoptic pattern falls into this category, and resembles Maddox et al.'s (1979) frontal-type flash flood event discussed earlier.

The socioeconomic impact of PREs is nonnegligible as documented by Rowe and Villarini (2013). They showed, using stream gauge data, that four of the six PREs over the Midwest during 2002–08 produced 10-yr flood events. Additionally, the PRE ahead of TC Erin (2007) produced the all-time Minnesota state record 24-h rainfall accumulation of 383.5 mm at Hokah, Minnesota, on 19 August (Galarneau et al. 2010; Schumacher et al. 2011; Schumacher and Galarneau 2012; Minnesota Department of Natural Resources 2015), while the PREs ahead of TCs Ike and Lowell (2008) set the all-time record daily rainfall of 189.5 mm at Lubbock, Texas, on 11 September; 261.9 mm at Wichita, Kansas, on 12 September; and 168.7 mm at Chicago–O'Hare, Illinois, on 13 September[1] (Bosart et al. 2012; Schumacher and Galarneau 2012).

The ability of operational numerical weather prediction systems to accurately forecast the occurrence, duration, and intensity of PREs is largely unknown. Examination of select individual cases has yielded mixed results. Galarneau et al. (2010) show that the PRE associated with TC Erin (2007) was well forecasted by the European Centre for Medium-Range Weather Forecasts ensemble prediction system, with 5-day forecasts indicating a 30% probability of over 50 mm of rainfall over the PRE region, increasing to a 90% probability in the 2-day forecast. A multimodel ensemble analysis of the TC Erin (2007) and
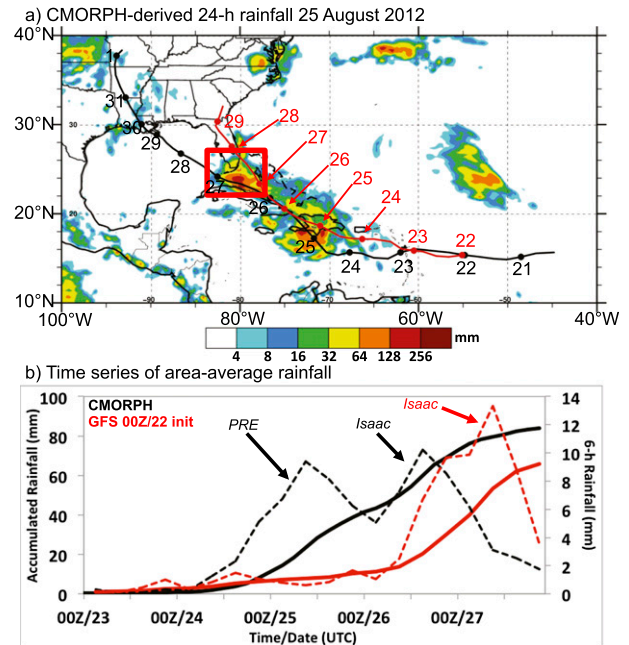

FIG. 1. (a) HURDAT (black; Landsea et al. 2004) and 0000 UTC 22 Aug 2012 GFS forecast (red) track of TC Isaac with filled circles marking the 0000 UTC positions and CMORPH-derived 24-h precipitation (shaded according to the color bar in mm) on 25 Aug 2012. (b) Time series of area-average 6-h precipitation (dashed; mm) and total accumulated precipitation (solid; mm) starting at 0000 UTC 23 Aug 2012 from CMORPH (black) and the GFS forecast (red) initialized at 0000 UTC 22 Aug 2012. The area average is computed in the red box shown in (a).

TC Ike (2008) PREs by Schumacher and Galarneau (2012) highlights the important challenges associated with the prediction of PREs. The first challenge is accurately predicting the TC track, since if the track is well forecasted then the moisture plume transport will likely be well forecasted. The second challenge is to obtain an accurate representation of the moisture field in the model initial conditions. The third challenge is to accurately predict the timing and intensity of the lifting mechanism (e.g., midlatitude trough, upper-level jet streak, and lower-level baroclinic zone) in which the heavy rainfall develops.

The present paper aims to examine a PRE that occurred over southern Florida on 25 August 2012 ahead of TC Isaac (2012) (Fig. 1). This case is unique compared to previously analyzed PREs over the CONUS (e.g., Galarneau et al. 2010; Schumacher et al. 2011; Bosart et al. 2012; Schumacher and Galarneau 2012; Moore et al. 2013) and eastern Asia (e.g., Wang et al. 2009; Byun and Lee 2012; Meng and Zhang 2012; Baek et al. 2013) documented in the refereed literature, as it occurred in subtropical latitudes and directly influenced the track of a TC by modifying the TC steering flow. In the case of TC Isaac, PRE-induced convectively driven divergent outflow

---

[1] The all-time record daily rainfall at Chicago–O'Hare, Illinois, was eclipsed on 23 July 2011 with 174.2 mm (Bosart et al. 2012).

contributed to thinning and fracture of an upper-level trough over Florida, which allowed Isaac to move northwestward into the Gulf of Mexico rather than recurve into Florida. Medium-range TC track forecasts from the operational National Centers for Environmental Prediction (NCEP)–Global Forecast System (GFS) recurved Isaac over and east of Florida rather than continued Isaac northwestward into the Gulf of Mexico. As an example, the GFS forecast initialized at 0000 UTC 22 August 2012 is compared to the observed track in Fig. 1a. We will show that early recurvature in the GFS forecasts is linked to the model's inability to predict the occurrence of the PRE ahead of Isaac (Fig. 1b). This study highlights the complex interaction between a PRE and its environment and how that impacts a TC threatening the U.S. mainland, thus posing a significant forecast challenge.

This study is organized as follows. Section 2 describes the data and diagnostic calculations used to analyze the PRE. Section 3 provides an overview of Isaac and the PRE and diagnosis of the PRE's importance in the track of Isaac, while section 4 analyzes track forecasts for Isaac from the deterministic GFS. The conclusions are provided in section 5.

2. Data and methods

The NCEP GFS analyses and forecasts are available 4 times daily at $0.5° \times 0.5°$ horizontal grid spacing on isobaric levels at 50-hPa increments (25 hPa below 750 hPa), and constitutes the primary data source for this study. These data are supplemented by National Aeronautics and Space Administration (NASA) Geostationary Operational Environmental Satellite (GOES)-East infrared satellite imagery and upper-level radiosonde observations. Precipitation analyses are generated using the NOAA Climate Prediction Center Morphing Technique (CMORPH; Joyce et al. 2004) 3-h global precipitation analyses available at ~8-km horizontal grid spacing. Air parcel trajectories are computed using the NCEP GFS analyses at 6-h intervals, with linear interpolation used at 1-h intervals between analysis times.

Diagnostic calculations used herein include the vertically integrated water vapor transport (IVT; Moore et al. 2012), calculated as

$$IVT = -\int_{P_0}^{p} (q\mathbf{V})\frac{dp}{g}, \quad (1)$$

where p_0 is 1000 hPa, p is 300 hPa, $\mathbf{V}$ is the the horizontal wind vector, q is the water vapor mixing ratio, and g is the acceleration due to gravity, and Petterssen frontogenesis (Keyser et al. 1986), defined as

$$\frac{d}{dt_h}|\mathbf{\nabla}_h\theta| = -\frac{1}{2}|\mathbf{\nabla}_h\theta|(D_h - F_h\cos2\beta_h), \quad (2)$$

where h represents the horizontal plane and the quantities D_h and F_h denote the divergence and resultant deformation, respectively. The angle β_h is defined as the difference between the angles of the local orientation of the axis of dilatation and the isentropes in the horizontal plane.

The filamentation time τ_{fil} is applied to quantify the impact of the PRE on the evolution of an upper-level trough, and is defined as

$$\tau_{fil} = 2(E_{sh}^2 + E_{st}^2 - \zeta^2)^{-1/2}, \quad (3)$$

where E_{sh} is the shearing deformation, E_{st} is the stretching deformation, and ζ is the relative vorticity. The τ_{fil} represents the e-folding time for filamentation of vorticity structures as derived by Rozoff et al. (2006). Physically, vorticity structures elongate in regions where the resultant deformation , $E_{sh}^2 + E_{st}^2$ is larger than the rotational flow ζ^2 [see Riemer and Jones (2014), their section 6.1]. A divergent filamentation time is also used to determine the impact of divergent outflow associated with the PRE on the structure of an upper-level trough. The filamentation time due to divergent flow [τ_{fil}^{div}; Riemer and Jones (2014), their Eq. (7)] is defined as

$$\tau_{fil}^{div} = \frac{(1 - 1/e)L_x}{u_{div}}, \quad (4)$$

where L_x is the length scale and u_{div} is the component of the divergent wind normal to the trough axis.

Vorticity inversion is used to compute the environmental wind in which TC Isaac is embedded with the effect of Isaac's cyclonic circulation removed. To do so, we follow the methodology of Galarneau and Davis (2013; see also Davis et al. 2008), where the streamfunction and velocity potential are computed as

$$\nabla^2\psi = \begin{pmatrix} \zeta & \text{for} & r \leq r_0 \\ 0 & \text{for} & r > r_0 \end{pmatrix} \quad (5)$$

and

$$\nabla^2\chi = \begin{pmatrix} \delta & \text{for} & r \leq r_0 \\ 0 & \text{for} & r > r_0 \end{pmatrix}, \quad (6)$$

where ψ is the streamfunction, χ is the velocity potential, ζ is the relative vorticity, δ is the divergence, and r_0 is the radius at which the TC is removed. From the solutions of (5) and (6), we can determine the nondivergent and divergent wind vectors from

$$\mathbf{V}_\psi = \mathbf{k} \times \nabla\psi \qquad (7)$$

and

$$\mathbf{V}_\chi = \nabla\chi. \qquad (8)$$

The environmental wind with the effect of the TC removed for a given radius r_0 is then computed as

$$\mathbf{V}_{\text{env}} = \mathbf{V} - \mathbf{V}_\psi - \mathbf{V}_\chi, \qquad (9)$$

where $\mathbf{V}_{\text{env}}$ is the environmental wind vector and $\mathbf{V}$ is the total wind. The steering layer flow is then defined as the area (r_0 can range from 1° to 8°) and vertically (depth can range from the 850–800- to 850–200-hPa layer) averaged $\mathbf{V}_{\text{env}}$ that best matches the TC motion based on positions at ± 12 h (Galarneau and Davis 2013, 409–410).

3. Analysis of PRE and track of Isaac

a. Overview and moisture sources

Tropical Cyclone Isaac originated as an African easterly wave over the tropical North Atlantic in mid-August 2012. Isaac reached tropical storm intensity late on 21 August, and moved into the eastern Caribbean on 23 August (Fig. 1). On 25 August, Isaac turned northwestward and moved over the southwest corner of Haiti to the north side of Cuba. Isaac continued on its northwestward course through the Straits of Florida into the Gulf of Mexico on 26–27 August, intensified to category-1 intensity on the Saffir–Simpson scale (Simpson 1974) on 28 August, and made landfall over southeast Louisiana on 29 August. A summary of Isaac's life cycle was provided by Berg (2013).

The 24-h CMORPH-derived rainfall for 25 August 2012 is shown in Fig. 1a. While Isaac moved from the south of Hispaniola to the north side of Cuba, heavy rainfall over 100 mm occurred over the Straits of Florida. Rain gauge observations over southern Florida recorded 40–100 mm of rainfall, with the highest amount near the coastal regions of southeast Florida (not shown). This region of rainfall occurred ahead of Isaac and was separate from the rain shield in Isaac's cyclonic circulation (Fig. 1a). The time series of area-averaged rainfall within the box in Fig. 1a shows that there were two peaks in 6-h rainfall during 23–28 August (Fig. 1b). The initial peak occurred on 25 August when Isaac was still in the Caribbean and the second occurred on 26 August in conjunction with the passage of Isaac into the Gulf of Mexico. The GOES-East infrared satellite imagery showed that deep convection developed and aggregated into a coherent mesoscale precipitation system between southeast

Florida and northern Cuba just after 0000 UTC 25 August (Figs. 2a,b). The convective system remained nearly stationary on 25 August and was clearly separated from the main cloud shield associated with Isaac (Figs. 2b–d). Isaac merged with the precursor convective system on 26 August as it moved northwestward into the Gulf of Mexico (not shown).

At 0000 UTC 24 August, Isaac was located over the eastern Caribbean on the equatorward flank of the oceanic subtropical anticyclone while an upper-level trough was located over the southeast United States and the eastern Gulf of Mexico (Fig. 3a). The sounding at Key West, Florida (EYW), showed fairly dry conditions throughout the troposphere with 34 mm of total column precipitable water (PW; Fig. 4). The northern part of Isaac's tropical moisture plume was advected northwestward toward the Straits of Florida beginning at 1200 UTC 24 August in conjunction with 20 m s^{-1} low-level flow located between Isaac and the subtropical ridge to the north (Fig. 3b). The tropical moisture plume reached the developing mesoscale precipitation system southeast of EYW at 0000 UTC 25 August (Figs. 3c and 2b). The sounding at EYW also showed a marked increase in PW to over 50 mm in conjunction with moistening below 500 hPa (Fig. 4). The flow above 500 hPa backed and strengthened in the 24-h ending at 0000 UTC 25 August as the upper-level trough moved southeastward over Florida and into the eastern Gulf of Mexico (see also Figs. 3a–c).

By 1200 UTC 25 August the mature convective system southeast of Florida was embedded in deep tropical moisture with PW values approaching 60 mm (Figs. 3d and 4). The sounding at EYW at 1200 UTC 25 August showed that the convective system occurred along a midlevel frontal zone marked by an abrupt wind shift and temperature inversion near 400 hPa with warm advection aloft (Fig. 4). The midlevel frontal zone was a signature of the upper-level trough over Florida (Fig. 3d). On 26 August, Isaac moved through the Straits of Florida and into the Gulf of Mexico (Figs. 3e,f). Heavy precipitation continued with Isaac's passage (Fig. 1b), aided by deep tropical moisture and deep warm advection (Fig. 4). The ability of Isaac to continue northwestward was abetted by the thinning and fracture of the upper-level trough over Florida on 25–26 August (Figs. 3c–f). In all, the rainfall associated with the precursor mesoscale precipitation system and Isaac resulted in widespread flooding over southern Florida (Berg 2013).

The precursor mesoscale precipitation system was a rainstorm separate from Isaac that produced over 100 mm in 24 h (Figs. 1 and 2). Analyses of PW suggested that moisture that reached the rainstorm originated from the Isaac moisture plume (Fig. 3). These conditions
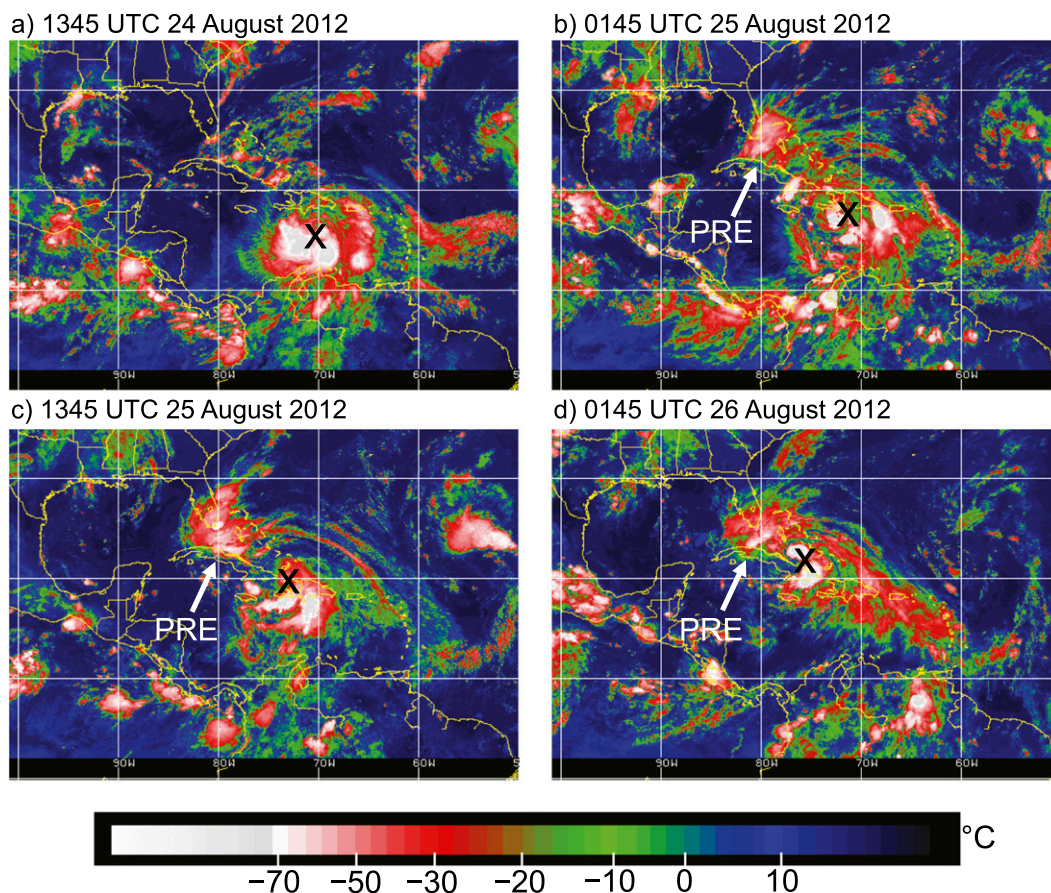
FIG. 2. GOES-East color enhanced (shaded according to the color bar in °C) infrared satellite imagery valid at (a) 1345 UTC 24 Aug, (b) 0145 UTC 25 Aug, (c) 1345 UTC 25 Aug, and (d) 0145 UTC 26 Aug 2012. The position of TC Isaac is marked with an X and the PRE is labeled with a white arrow. Imagery was obtained from CIMSS.

indicate that the precursor rainstorm was indeed a PRE. This assertion was supported by IVT and air parcel trajectory analyses shown in Fig. 5. The time-mean IVT for 1200 UTC 23–25 August showed a maximum that extended from north of Isaac to the PRE region (Fig. 5a). The air parcel trajectory analysis supported the IVT calculation, indicating that approximately 50% of air parcels that ended in the PRE region at 1500 and 3000 m above mean sea level at 0000 UTC 25 August originated within the Isaac moisture plume at 0000 UTC 23 August (Fig. 5b). The air parcels at 9000 m originated on the west side of the upper-level trough over the eastern third of the United States. The air parcels at all levels initially descended through 0000 UTC 24 August, followed by gradual ascent in the 24 h before 0000 UTC 25 August as they approached the PRE region (Fig. 5c). The air parcels in the mid- and upper levels moistened as they ascended, while the low-level air parcels remained moist (relative humidity values ≥75%) throughout the 48-h period (Fig. 5d).

b. Evolution of circulation features and lifting mechanisms

The evolution of key subsynoptic-scale circulation features during 1200 UTC 23–26 August 2012 is shown in Fig. 6. The symbols used to identify key circulation features are summarized in Table 1. At 1200 UTC 23 August, Isaac was located over the eastern Caribbean, while an upper-level trough (T_1) extended from eastern Cuba northward to 30°N and a second upper-level trough (T_2) was located over the southeast United States and was contributing to extratropical cyclone (C) development along the southeast U.S. coast (Fig. 6a). By 1200 UTC 24 August, development of C continued along the southeast U.S. coast while a subtropical ridge developed downstream over the western North Atlantic (Fig. 6b). Upper-level trough T_1 weakened in the north–south deformation zone (not shown) between developing cyclone C and subtropical ridge A. Well-defined low-level southeasterly flow formed between Isaac and subtropical
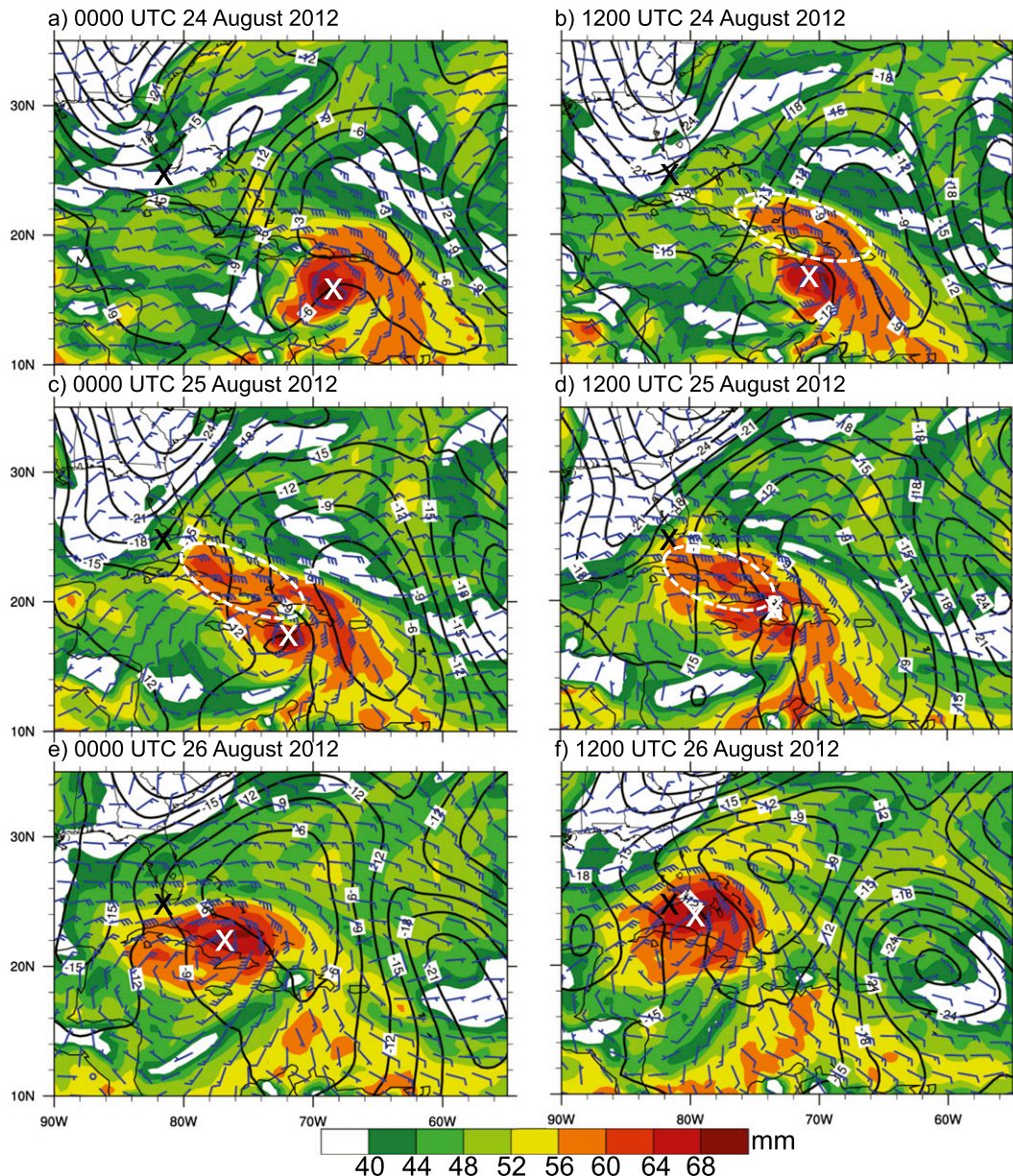
FIG. 3. GFS analysis total column PW (shaded according to the color bar in mm), 250-hPa streamfunction (black contours every $3 \times 10^6 \, m^2 \, s^{-1}$), and 850–700-hPa layer-mean wind vector (half barb = $2.5 \, m \, s^{-1}$; full barb = $5.0 \, m \, s^{-1}$; pennant = $25.0 \, m \, s^{-1}$) at (a) 0000 UTC 24 Aug, (b) 1200 UTC 24 Aug, (c) 0000 UTC 25 Aug, (d) 1200 UTC 25 Aug, (e) 0000 UTC 26 Aug, and (f) 1200 UTC 26 Aug 2012. The location of EYW and TC Isaac are marked by a black and white X, respectively. The tropical moisture plume ahead of Isaac is marked by a white-dashed unfilled ellipse in (b)–(d).

ridge A and a region of low-level cyclonic vorticity (P) formed over Cuba on the cyclonic-shear-side of the low-level flow.

The low-level cyclonic vorticity feature P moved northwestward and amplified south of Florida in conjunction with the PRE by 1200 UTC 25 August (Figs. 2c and 6c). At the same time, upper-level trough T_2 began to thin and fracture from the northern part of the trough through 1200 UTC 26 August (Figs. 6c,d). Concurrently,

the low-level cyclonic vorticity P that amplified in conjunction with the PRE began to interact with Isaac. The binary interaction (Fujiwhara 1923, 1931; Dong and Neumann 1983) between Isaac and cyclonic vorticity P, combined with thinning and fracture of upper-level trough T_2, led to Isaac tracking northwestward into the Gulf of Mexico by 1200 UTC 26 August (Fig. 6d). More detailed diagnosis of the impact of the PRE on the upper-level trough and Isaac's motion will be presented in section 3c.
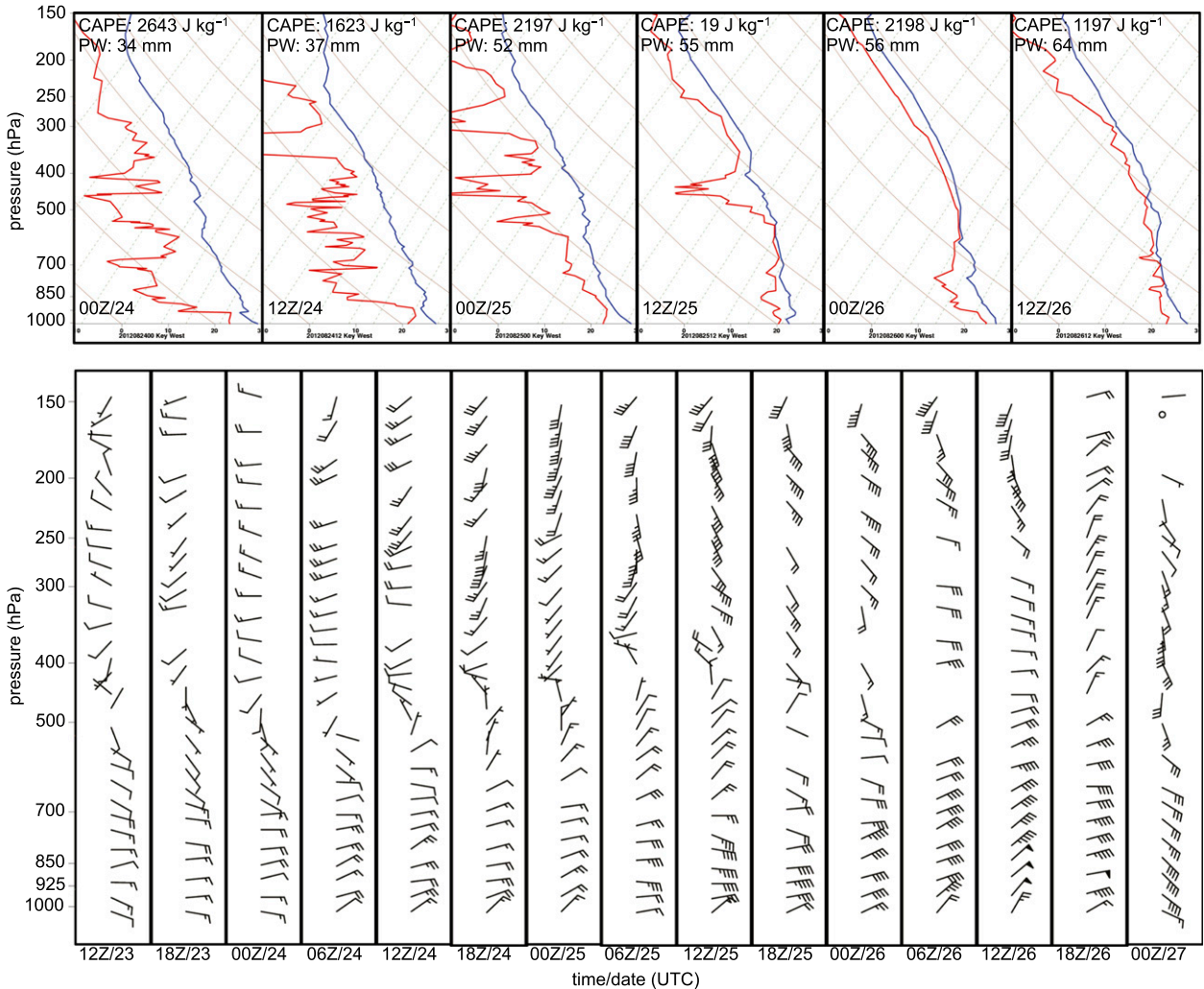
FIG. 4. Sequence of skew T–log$p$ diagrams of (top) air temperature (°C; blue) and dewpoint (°C; red), and (bottom) wind vector (barbs as in Fig. 3) for EYW at 1200 UTC 23 Aug–0000 UTC 27 Aug 2012. The vector wind profiles are shown every 6 h starting at 1200 UTC 23 Aug, and the thermodynamic profiles every 12 h starting at 0000 UT 24 Aug. The convective available potential energy (CAPE; J kg^{-1}) and total column PW (mm) are indicated on each thermodynamic profile.

To examine the lifting mechanisms and physical processes that contributed to PRE formation, vertical cross sections of water vapor mixing ratio, potential temperature (θ), flow in the plane of the cross section, and potential vorticity [PV; PV unit (PVU), 1 PVU = 10^{-6} K kg^{-1} m^2 s^{-1}], θ, and wind are shown in Fig. 7. At 0000 UTC 25 August, the developing PRE was located on the leading edge of the plume of deep tropical moisture extending northwestward from Isaac (Figs. 7a,b and 3c). A region of ascent was located on the warm, moist southeast side of an axis of mid- to upper-level frontogenesis in a region of deformation (shown by streamfunction contours in Fig. 7a) on the southeast flank of upper-level trough T$_2$ (Figs. 7b,c). The environment was also characterized by deep warm air advection on the leading flank of

low-level cyclonic vorticity feature P. The PRE matured on the leading edge of the deep tropical moisture in a region of synoptic forcing for ascent associated with frontogenesis and warm advection by 1200 UTC 25 August (Fig. 7d). The low-level cyclonic vorticity feature P amplified in the presence of the PRE and began to interact with Isaac approaching from the southeast (Fig. 7e).

c. Impact of PRE on environment flow and Isaac's track

This subsection will examine the impact of the PRE on the environment flow and Isaac's motion. The bulk upscale effect of deep convection on upper-level trough T$_2$ over Florida on 25 August is shown in Fig. 8. A region
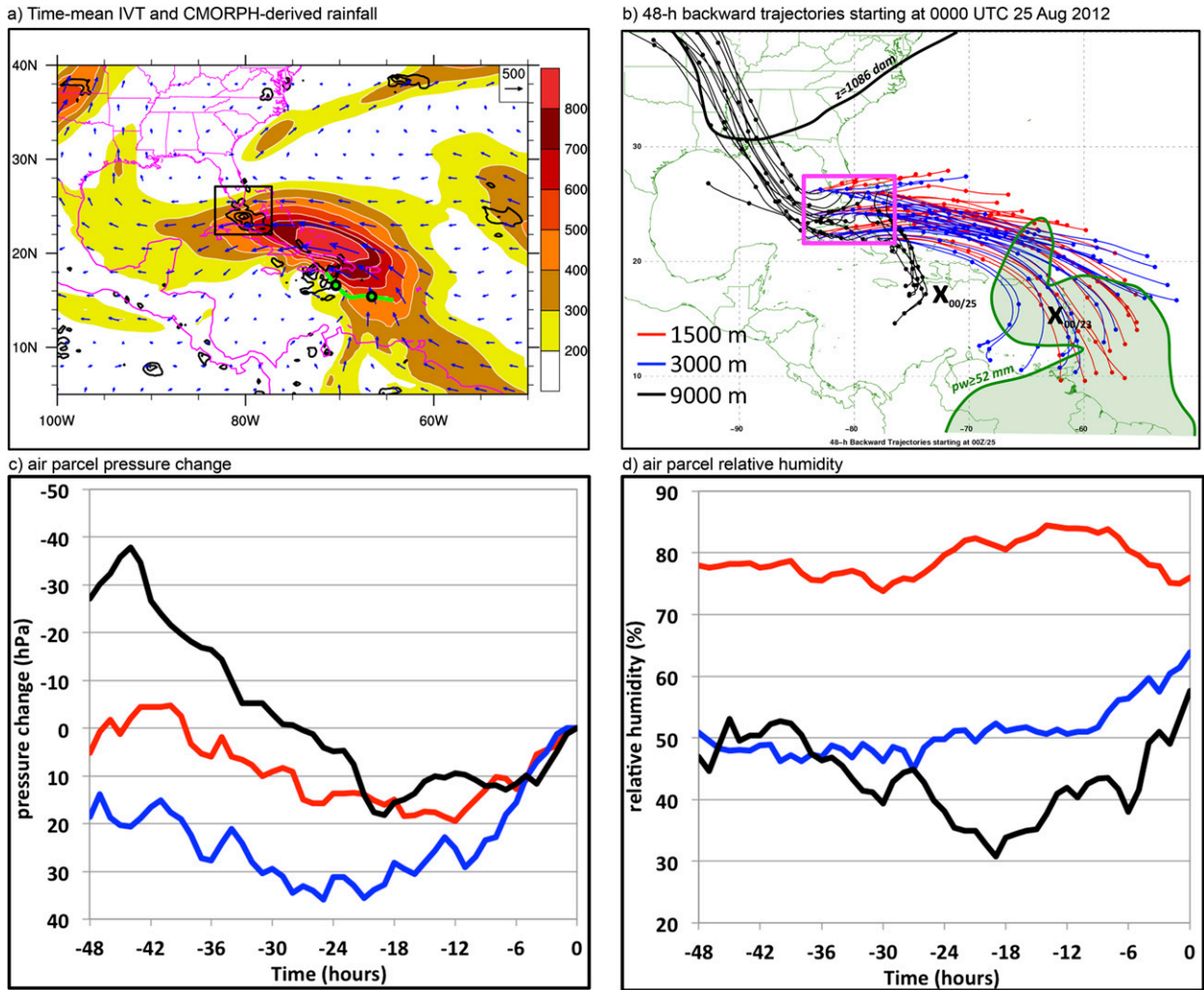
FIG. 5. (a) Time mean IVT vector (arrows with magnitude shaded according to the color bar in $kg\,m^{-1}\,s^{-1}$) and track of TC Isaac (green line with 0000 UTC positions marked by green-filled black circles) for 1200 UTC 23–25 Aug 2012 and CMORPH-derived 24-h precipitation (black contours at 50, 100, 150, and 200 mm) on 25 Aug 2012. (b) Forty-eight 48-h backward air parcel trajectories starting in the magenta box at 0000 UTC 25 Aug 2012. IVT vectors and trajectories are derived from the GFS analysis. The red, blue, and black air parcel trajectories start at 1500, 3000, and 9000 m above mean sea level, respectively. The position of Isaac at 0000 UTC 23 Aug and 25 Aug is marked with an X, and PW $\geq$ 52 mm at 0000 UTC 23 Aug is marked with a dark green line enclosing a light green shaded area. The 1086-dam 250-hPa geopotential height contour at 0000 UTC 23 Aug 2012 is marked by the thick black contour. The time series of the median air parcel pressure perturbation (hPa) relative to its value at 0000 UTC 25 Aug and relative humidity (%) are shown in (c) and (d), respectively.

of 600–400-hPa layer-mean ascent, the signature of the PRE in the GFS analyses, moved slowly northwestward on the north side of Cuba on 25 August. By 0600 UTC 25 August, upper-level divergent outflow associated with the PRE was impacting the southeast flank of the upper-level trough T_2 (Fig. 8b). The upper-level trough markedly thinned between 0600 and 1200 UTC 25 August as southeasterly divergent outflow slowed the progression of the forward flank of the trough through negative PV advection by the divergent wind (Figs. 8b,c). The attendant increase in PV gradient on the forward flank of the trough was coincident with strengthening of

the upper-level jet to the north. The divergent outflow helped to "lock in" the upper-level jet entrance region, maintaining the favorable synoptic-scale region of ascent. The role of convectively driven divergent outflow in "locking in" a favorable synoptic-scale environment for heavy rainfall was also documented in the PREs ahead of TC Ike by Bosart et al. (2012). By 1800 UTC 25 August, the upper-level trough T_2 was beginning to fracture in the presence of $\sim$5 m s^{-1} convectively driven divergent outflow associated with the PRE (Fig. 8d).

The filamentation time τ_{fil} was computed to assess the role of the PRE in the deformation and fracture of the
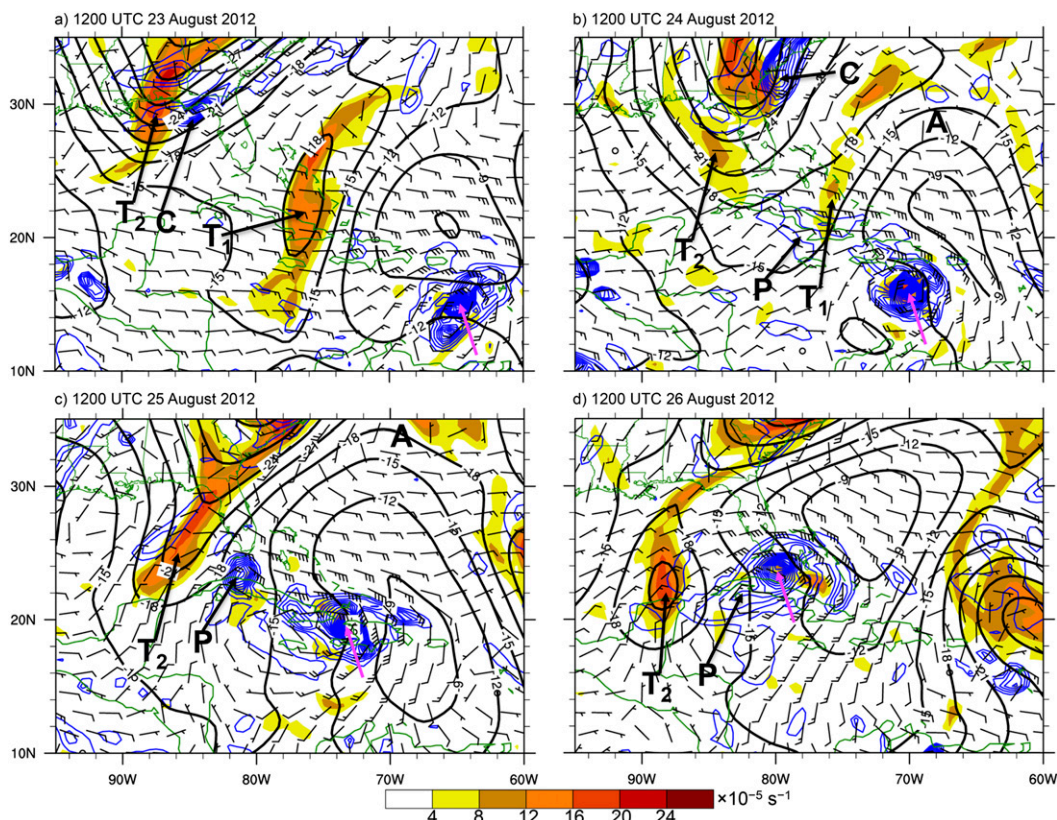
FIG. 6. GFS analysis 300–200-hPa layer-mean relative vorticity (shaded according to the color bar in $\times 10^{-5}\,\mathrm{s}^{-1}$) and streamfunction (black contours every $3.0 \times 10^{6}\,\mathrm{m}^{2}\,\mathrm{s}^{-1}$), and 700–500-hPa layer-mean relative vorticity (blue contours every $2.0 \times 10^{-5}\,\mathrm{s}^{-1}$ starting at $2.0 \times 10^{-5}\,\mathrm{s}^{-1}$) and wind vector (barbs as in Fig. 3) at (a) 1200 UTC 23 Aug, (b) 1200 UTC 24 Aug, (c) 1200 UTC 25 Aug, and (d) 1200 UTC 26 Aug 2012. Key circulation figures are labeled using the notation in Table 1. Isaac is marked by a magenta arrow.

upper-level trough over Florida (Fig. 9a). The computation of τ_{fil} at 1200 UTC 25 August showed low values $<0.25\,\mathrm{day}^{-1}$ along the trough axis just west of Florida (Fig. 9a), indicating that the synoptic-scale flow favored rapid thinning and elongation of the trough, leading to its eventual fracture. To assess the trough filamentation time due to the convectively driven divergent outflow associated with the PRE, we computed the divergent filamentation time $\tau_{\mathrm{fil}}^{\mathrm{div}}$ as in Riemer and Jones (2014, see their section 6.3). Figure 9b shows the 300–200-hPa layer-mean cyclonic relative vorticity and PRE-driven divergent outflow[2] at 1200 UTC 25 August (Fig. 9b). Using a divergent outflow normal to the trough axis of $3.3\,\mathrm{m\,s}^{-1}$ and a length scale of $400\,\mathrm{km}$, $\tau_{\mathrm{fil}}^{\mathrm{div}} \approx 0.9\,\mathrm{day}^{-1}$, indicating that the PRE-driven divergent outflow was a bit larger than the filamentation time with the full wind. Nonetheless, it is apparent that the PRE-driven

divergent outflow did contribute to thinning and fracture of the upper-level trough T_2 over Florida prior to the arrival of Isaac.

To address the role of the PRE and fracture of the upper-level trough T_2 in the motion of Isaac as it approached southern Florida, vorticity inversion of relevant circulation features was employed to attribute the amount of flow driven in Isaac's environment to each circulation feature. The key circulation features identified

TABLE 1. List of unique symbols used in the figures to label synoptic-scale weather systems.

Description	Figures
Upper-level trough over eastern Cuba (T_1)	Figs. 6a,b
Upper-level trough over eastern Gulf of Mexico (T_2)	Figs. 6; 7c,e; 10a,b; and 16c
Midlevel vorticity maximum with PRE (P)	Figs. 6b–d; 7c,e; and 10a,b
Subtropical anticyclone (A)	Figs. 6b,c and 10a,b
Extratropical cyclone (C)	Figs. 6a,b

[2] The PRE-driven divergent wind was computed using the divergence within $4°$ of the PRE centroid.
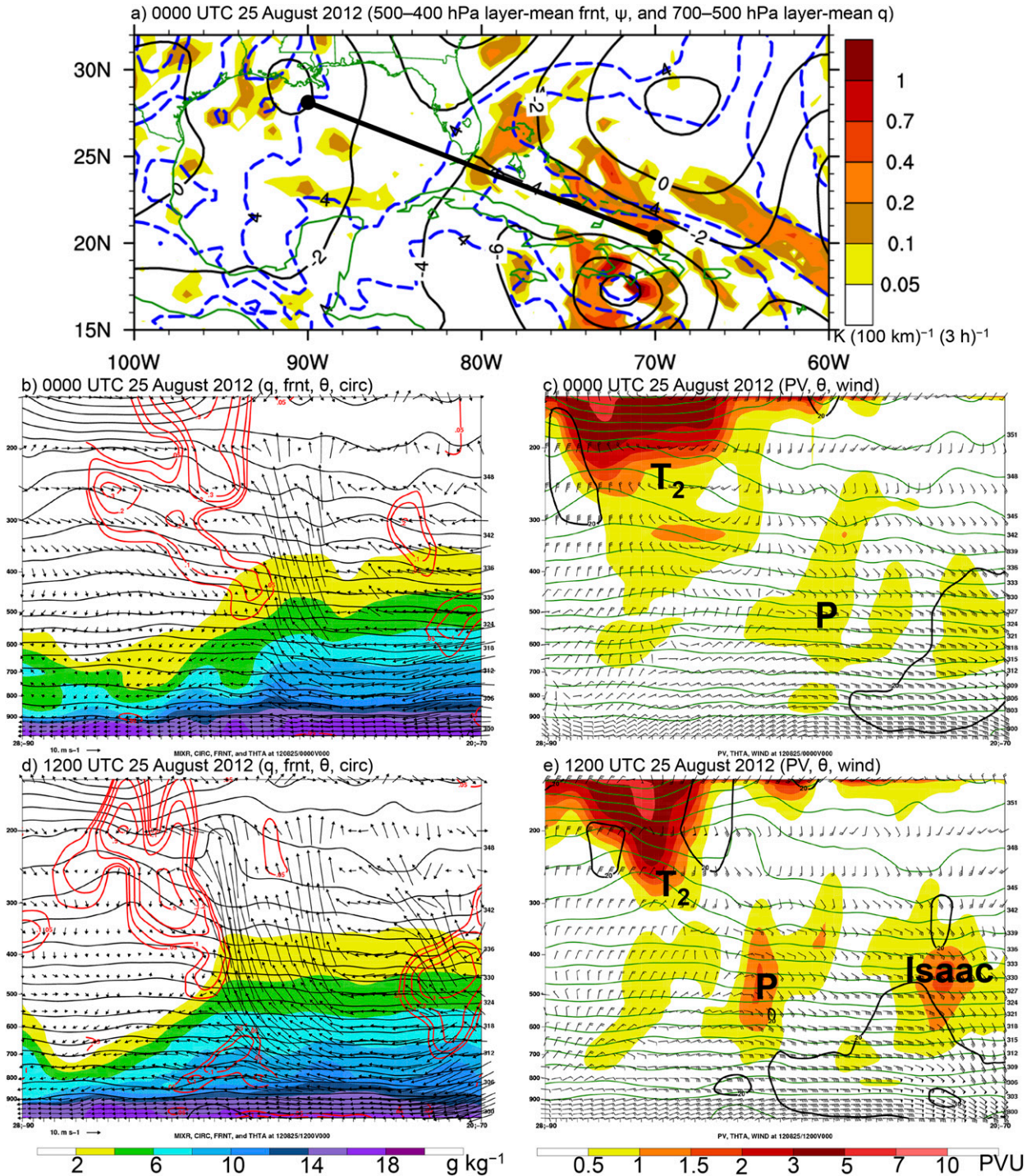
FIG. 7. GFS analysis (a) 500–400-hPa layer-mean streamfunction (black contours every $2.0 \times 10^6 \, \text{m}^2 \, \text{s}^{-1}$) and Petterssen frontogenesis [shaded according to the color bar to the right of (a) in K $(100 \, \text{km})^{-1} \, (3 \, \text{h})^{-1}$], and 700–500-hPa layer-mean water vapor mixing ratio (dashed blue contours every $2 \, \text{g kg}^{-1}$ starting at $4 \, \text{g kg}^{-1}$) at 0000 UTC 25 Aug 2012. Vertical cross sections [orientation plotted in (a) as solid black line] of water vapor mixing ratio [shaded according to the color bar beneath (d) in g kg^{-1}], potential temperature (black contours every 3 K), Petterssen frontogenesis [red contours at 0.05, 0.1, 0.2, 0.3, 0.4, and 0.5 K $(100 \, \text{km})^{-1} \, (3 \, \text{h})^{-1}$], and circulation in the plane of the cross section (arrows in m s^{-1} with scale located beneath left side of panel) at (b) 0000 and (d) 1200 UTC 25 Aug 2012. The PV [shaded according to the color bar beneath (e) in PVU], potential temperature (green contours every 3 K), and vector wind (barbs as in Fig. 3) at (c) 0000 and (e) 1200 UTC 25 Aug 2012.
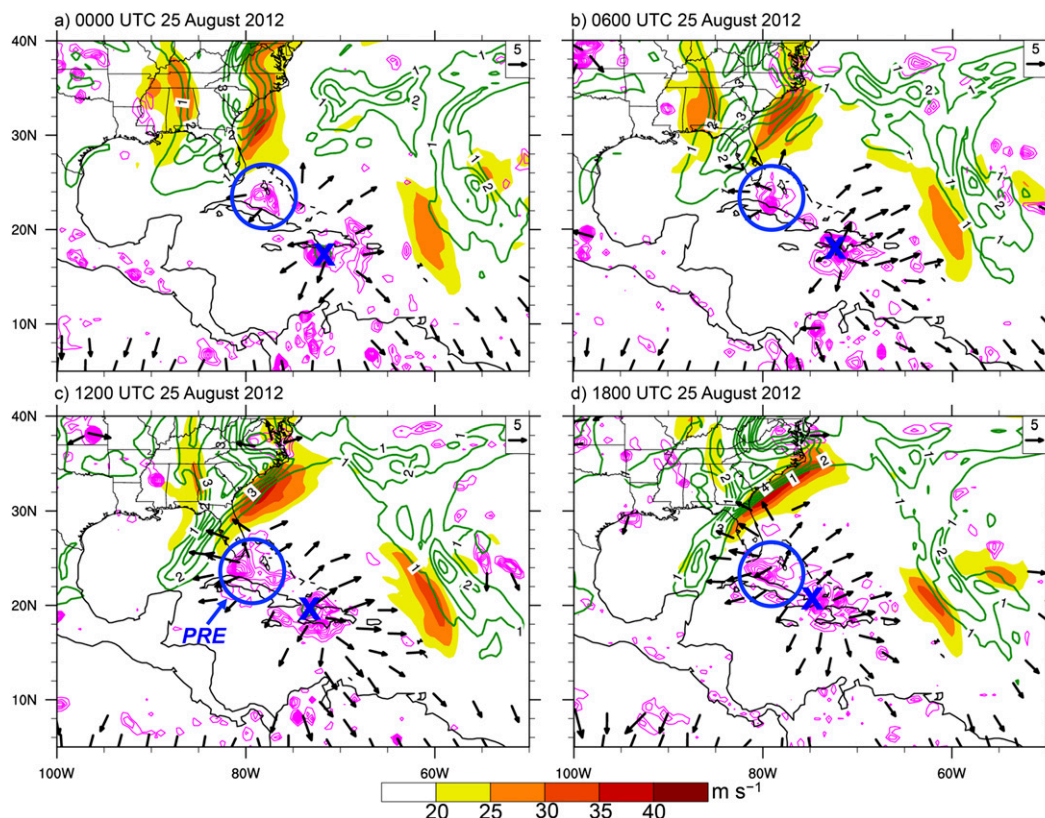
FIG. 8. GFS analysis 300–200-hPa PV (green contours every 1 PVU starting at 1 PVU), layer-mean divergent wind (arrows in m s^{-1} with scale at top right of each panel), layer-mean total wind speed (shaded according to the color bar in m s^{-1}), and 600–400-hPa layer-mean ascent (magenta contours every 0.3 Pa s^{-1} starting at -0.3 Pa s^{-1}) at (a) 0000, (b) 0600, (c) 1200, and (d) 1800 UTC 25 Aug 2012. The position of Isaac is marked by the blue X and the PRE is indicated by the blue unfilled circle.

include the (i) broad subtropical ridge over the western North Atlantic, (ii) circulation features over the Caribbean Sea, (iii) cyclonic vorticity associated with the PRE, (iv) cyclonic vorticity associated with the upper-level trough, and (v) near-storm vorticity asymmetries (Figs. 10a,b). The vorticity within each enclosed region marked in Fig. 10a was inverted to determine the 850–250-hPa layer-mean flow induced over Isaac by each of the five features listed above. The vorticity inversion revealed that the sub-tropical ridge induced an east-southeasterly flow over Isaac during 1200 UTC 25–26 August (Figs. 10c–e). This flow was balanced by the southerly flow induced by the cyclonic vorticity associated with the PRE and the upper-level trough and circulation features over the Caribbean Sea, and weak easterly flow on average from near-storm vorticity asymmetries, resulting in a $\mathbf{V}_{env}$ that steered Isaac through the Straits of Florida into the Gulf of Mexico. The residual difference between the actual storm motion and the total contribution from the five circulation features was due to a southwestward propa-gation component of Isaac's motion likely driven in part

by binary interaction between Isaac and the PRE cy-clonic vorticity after 1200 UTC 25 August (Figs. 6c,d and 10c).

4. Deterministic GFS track forecasts

a. 0000 UTC GFS forecasts

The track forecasts for TC Isaac from the operational GFS forecasts initialized at 0000 UTC 21 August–1 Sep-tember 2012 are shown in Fig. 11a. Forecasts initialized after 25 August accurately predicted landfall over the southeast Louisiana coastline on 29 August. Earlier ini-tializations, however, predicted an earlier recurvature for Isaac, with forecasts initialized on 21–22 August indicating recurvature over eastern Florida on 27 August. Fore-casts initialized on 23–25 August improved slightly, but still predicted an earlier recurvature and landfall over the Florida Panhandle on 29 August. After an initial departure in the forecast tracks from the observed track of Isaac over the eastern Caribbean Sea on 23–24 August,
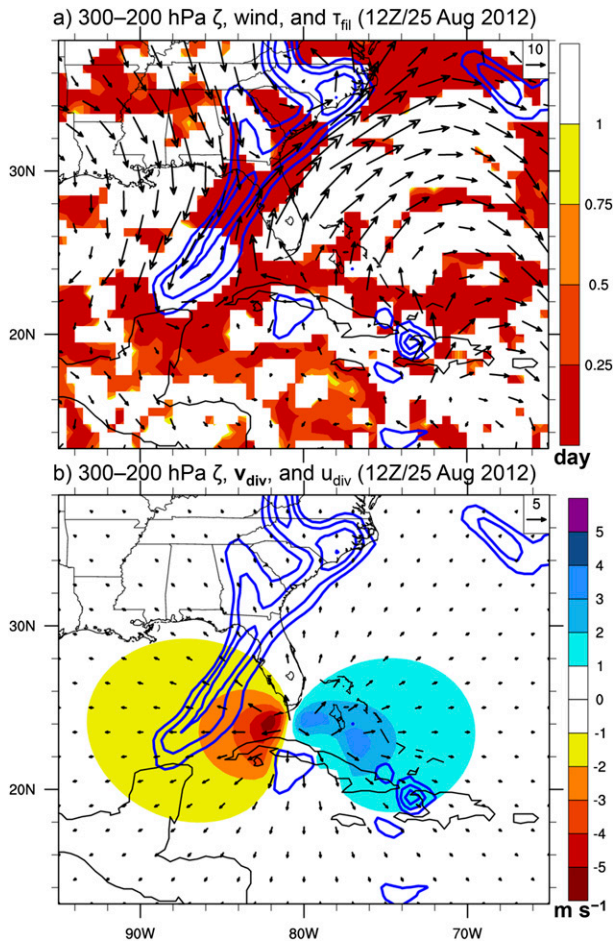
a) 300–200 hPa ζ, wind, and τ_fil (12Z/25 Aug 2012)

b) 300–200 hPa ζ, **v**_div, and u_div (12Z/25 Aug 2012)

FIG. 9. GFS analysis (a) 300–200-hPa layer-mean relative vorticity (blue contours every $4.0 \times 10^{-5}\,\mathrm{s}^{-1}$ starting at $4.0 \times 10^{-5}\,\mathrm{s}^{-1}$), wind vector (arrows in $\mathrm{m\,s}^{-1}$ with scale at top right of each panel), and τ_{fil} (shaded according to the color bar in units of day^{-1}), and (b) 300–200-hPa layer-mean relative vorticity (blue contours every $4.0 \times 10^{-5}\,\mathrm{s}^{-1}$ starting at $4.0 \times 10^{-5}\,\mathrm{s}^{-1}$), divergent wind vector (arrows in $\mathrm{m\,s}^{-1}$) due to divergence within 4° of the PRE center, and the zonal component of divergent wind (shaded according to the color bar in $\mathrm{m\,s}^{-1}$) at 1200 UTC 25 Aug 2012.

the final departure occurred on 26 August as the forecasted tracks initialized at 0000 UTC 21–25 August moved on a more northward course (Fig. 11a).

Comparison of the absolute track errors for Isaac from the GFS forecasts initialized at 0000 UTC 21–25 August 2012 with the GFS mean absolute error for TCs over the North Atlantic basin during 2012–14 and the Hurricane Forecast Improvement Project (HFIP) track error baseline[3] is shown in Fig. 11b. The track

[3] The HFIP track error baseline was computed from the top-flight operational models for the 2006–08 North Atlantic TC seasons (Gall et a. 2014).

forecast errors for Isaac were comparable or lower than the 2012–14 climatology at 1200 UTC 26 August (time of "early recurvature" marked by arrows), and generally increased thereafter. While the medium-range track forecast errors for Isaac were consistent with the 2012–14 statistics, they were higher than the HFIP baseline by 168 h.

Comparison of 300–200-hPa layer-mean ζ and ψ and 700–500-hPa layer-mean ζ and wind between the GFS forecasts and the verifying GFS analysis at 0000 UTC 26 August (just prior to the departure in track forecasts from the observed) is shown in Fig. 12. The GFS forecasts initialized at 0000 UTC 21–22 August were characterized by a larger upper-level trough over the southeast United States and increased westerly flow aloft over Florida and the western North Atlantic compared to the analysis at 0000 UTC 26 August (Figs. 12a,b,f). The southwest end of the analyzed upper-level trough was beginning to fracture and move southwestward, while the forecasted trough shows no evidence of thinning and fracturing. The forecasts initialized at 0000 UTC 23–25 August placed the core of the upper-level trough farther northeast in agreement with the verifying analysis (Figs. 12c–f). The forecasts on 23–24 August both showed a thin upper-level trough structure that extended southwestward from the core of the trough over the Carolina coast into the Gulf of Mexico, but with no evidence of fracturing as in the analysis (Figs. 12c,d,f). The forecast initialized at 0000 UTC 25 August showed indication that the upper-level trough was fracturing over the Gulf of Mexico (Fig. 12e).

Also of interest was the position of the upper-level anticyclone northeast of Isaac. For forecasts initialized at 0000 UTC 21–23 August, the anticyclone was positioned east and northeast of Isaac and the upper-level southwesterly flow was located over Florida and the western North Atlantic (Figs. 12a–c). For initializations at 0000 UTC 24–25 August, the anticyclone expanded westward on the north side of Isaac (Figs. 12d,e). The increased ridging over Florida and the western North Atlantic, and fracture of the upper-level trough on the Gulf of Mexico, resulted in flow with an *easterly* component over southern Florida to Cuba, aiding in the more westward track of Isaac in the later initializations and verifying analysis (see also Fig. 12f).

The GFS forecasts of 300–200-hPa layer-mean PV, wind speed, vector divergent wind, and 600–400-hPa layer-mean ascent verifying at 1200 UTC 25 August is shown in Fig. 13. The GFS forecasts initialized at 0000 UTC 21–24 August all failed to predict the PRE ahead of Isaac over the Straits of Florida on 25 August (Figs. 13a–d and 8c). The GFS forecast initialized at
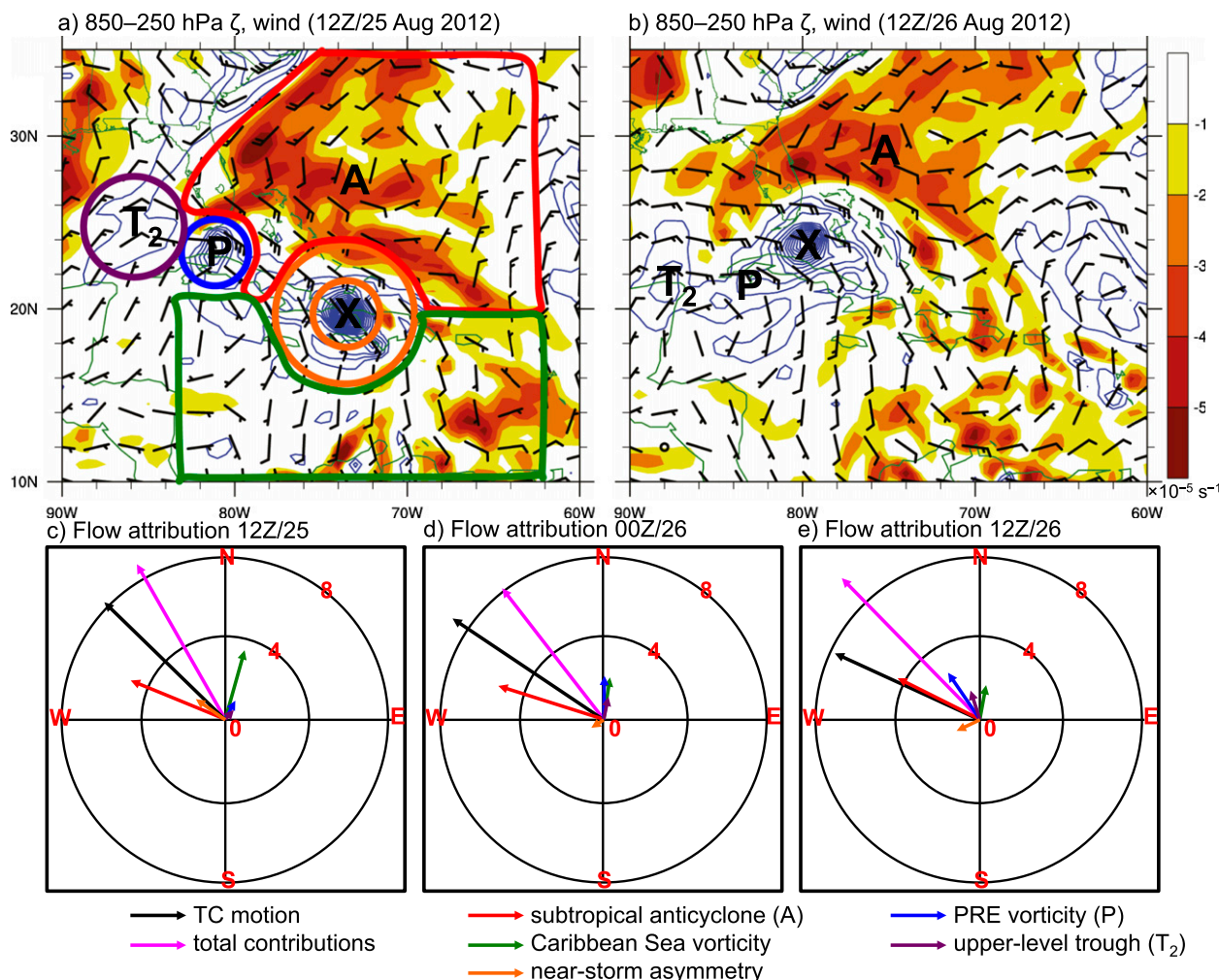
FIG. 10. GFS analysis 850–250-hPa layer-mean $\mathbf{V}_{env}$ (barbs as in Fig. 3) (TC Isaac removed using $r_0 = 2°$) and relative vorticity (anticyclonic shaded according to the color bar in $\times 10^{-5}\,\mathrm{s}^{-1}$; cyclonic contoured in blue every $2.0 \times 10^{-5}\,\mathrm{s}^{-1}$ starting at $2.0 \times 10^{-5}\,\mathrm{s}^{-1}$) at 1200 UTC (a) 25 Aug and (b) 26 Aug 2012. The location of Isaac is marked with an X. The key synoptic-scale circulation features are marked by unfilled shapes and symbols defined in Table 1. Vorticity inversion is used to compute the flow over Isaac induced by vorticity within each unfilled shape. The red region covers the broad subtropical ridge over the western North Atlantic, the green region is for the Caribbean Sea vorticity, the blue circle indicates the cyclonic vorticity associated with the PRE, and purple circle shows the cyclonic vorticity associated with the upper-level trough. The near-storm vorticity asymmetry is measured by vorticity in the 2°–4° radial band indicated by the unfilled orange circles. The flow $(\mathrm{m\,s}^{-1})$ associated with these synoptic circulation features for (c) 1200 UTC 25 Aug, (d) 0000 UTC 26 Aug, and (e) 1200 UTC 26 Aug 2012 is shown. The actual TC motion and sum of the contributions from all the circulation features is also plotted in black and magenta, respectively.

0000 UTC 25 August was the first to represent the PRE and the subsequent upper-level trough fracture on 26 August (Figs. 13e and 12e). This result suggested a strong linkage between the PRE and fracture of the upper-level trough over Florida, which impacted the track of Isaac on 26–29 August. In section 4b, the GFS forecast initialized at 0000 UTC 22 August will be diagnosed in more detail to determine how the missed PRE and upper-level trough fracture contributed to the early recurvature of Isaac over eastern Florida on 26 August (Fig. 11).

b. Diagnosis of GFS forecast initialized at 0000 UTC 22 August 2012

The GFS track forecast initialized at 0000 UTC 22 August was characterized by an early recurvature error, with the forecast track turning on a more northward course compared to the observed track beginning at 1200 UTC 26 August (Fig. 14a). The GFS forecast track made landfall along the eastern Florida coast near 1800 UTC 27 August, while the observed track continued northwestward into the

a) 0000 UTC GFS track forecasts for Isaac
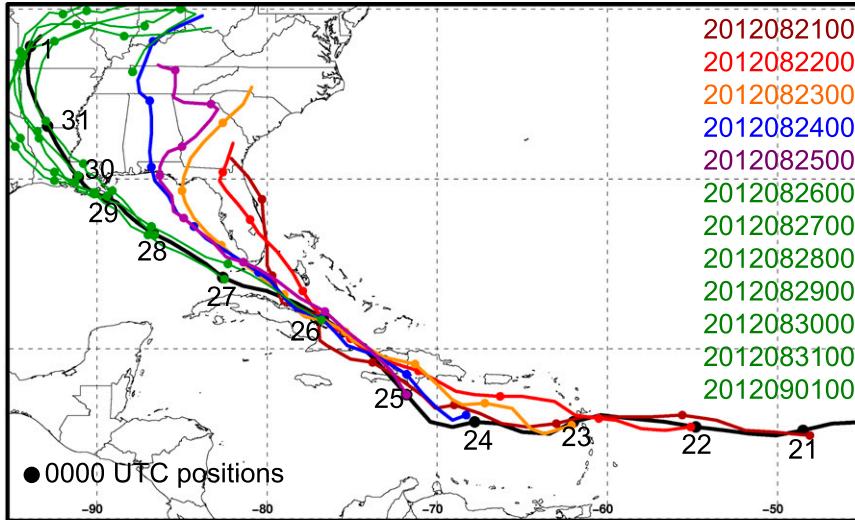
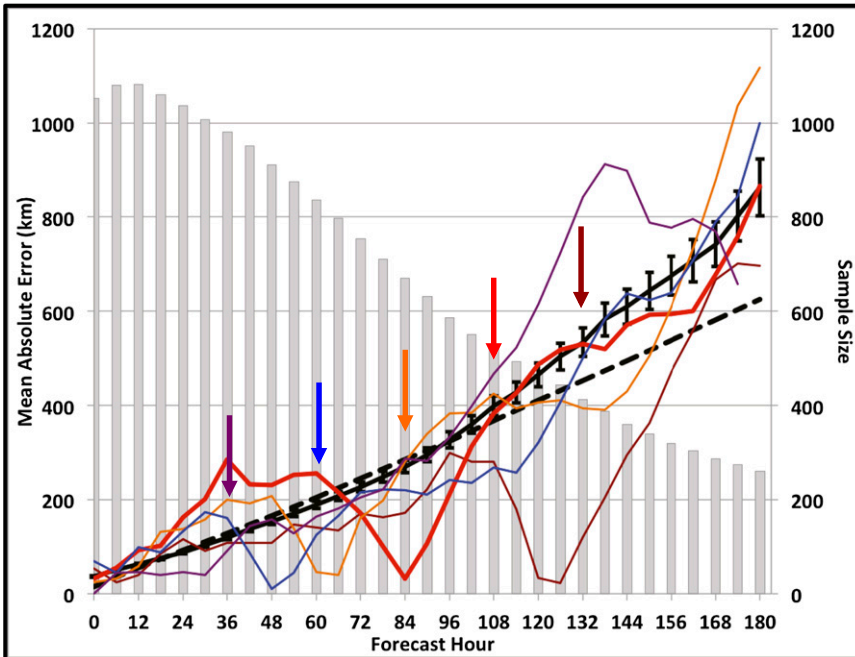b) GFS absolute track error for 2012–2014 and for Isaac

FIG. 11. (a) HURDAT (black line) and GFS (colored lines) track forecasts initialized at 0000 UTC 21 Aug–1 Sep 2012 for TC Isaac. The 0000 UTC positions are marked by filled circles. (b) The mean absolute track error (km; solid black line) for the operational GFS during 2012–14 in the North Atlantic, HFIP ''baseline'' track error (km; dashed black line), sample size (gray bars), and absolute track error for GFS forecasts of Isaac [same color convention as in (a)] initialized at 0000 UTC 21 Aug–25 Aug 2012. The error bars represent the 90% confidence interval. Arrows represent the verifying time of 1200 UTC 26 Aug 2012 for the individual Isaac forecasts, using the same color convention as in (a).

Gulf of Mexico making landfall over the southeast Louisiana coast on 29 August. Diagnosis of the track forecast error at 1200 UTC 26 August—the time in which the forecasted TC motion departed from

observed—shows that the GFS forecast $\mathbf{V}_{env}$ was characterized by a deep-layer westerly error that maximized at $\sim 6 \, \mathrm{m \, s^{-1}}$ at 600 hPa (Fig. 14b). The $\mathbf{V}_{env}$ error vertically integrated in the 850–250-hPa layer, defined here as
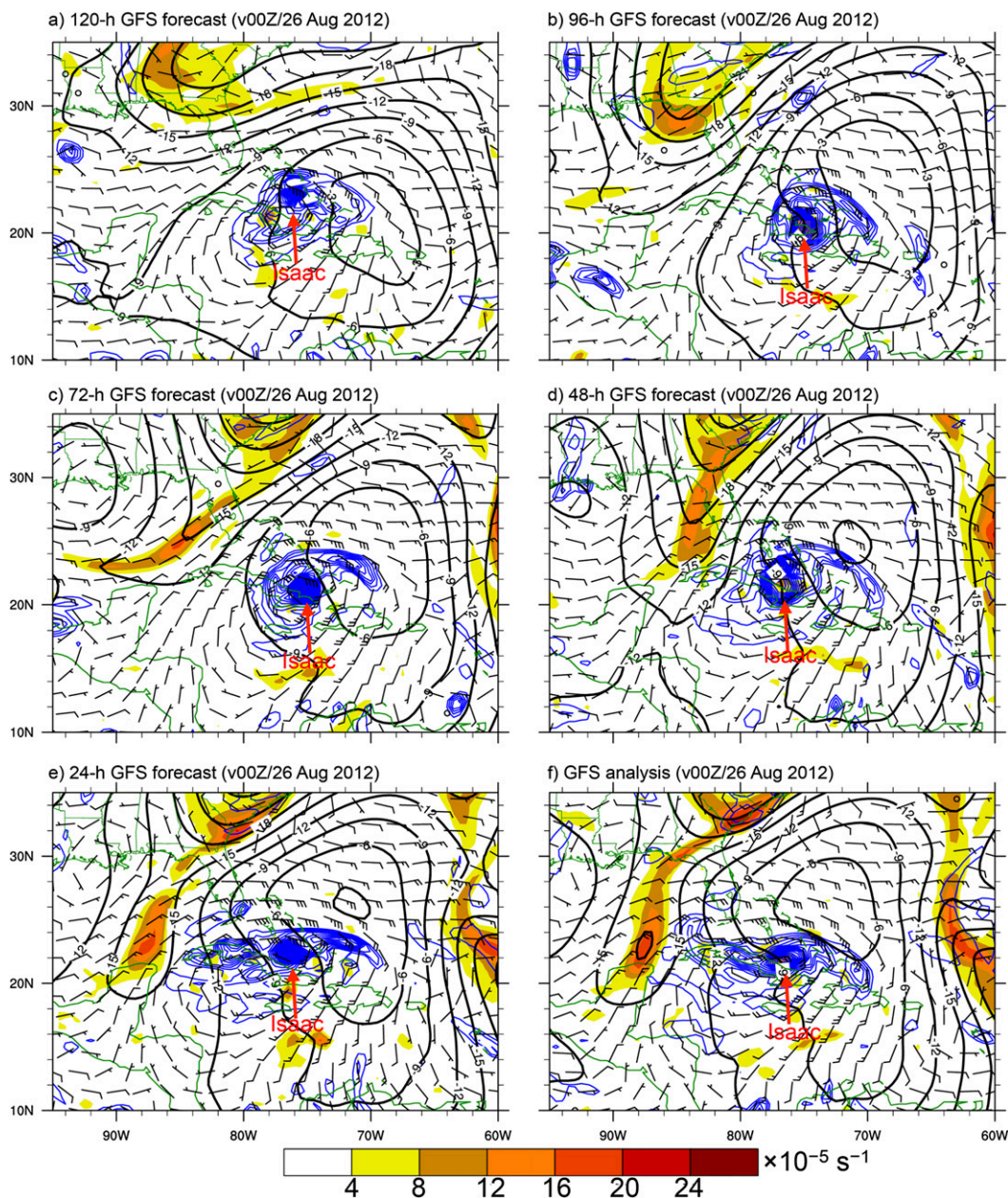
FIG. 12. As in Fig. 6, but for the (a) 120-, (b) 96-, (c) 72-, (d) 48-, and (e) 24-h GFS forecasts and (f) GFS analysis verifying at 0000 UTC 26 Aug 2012. TC Isaac is marked by a red arrow.

Isaac's steering layer,[4] shows that the westerly steering layer flow error was attributed to an anticyclonic circulation error south of Isaac and a cyclonic circulation error north of Isaac (Fig. 14c). The steering layer flow error and 600-hPa geopotential height and $\mathbf{V}_{env}$ error

maps are in TC-relative coordinates, with the TC located at the observed position and geography shown for scale (Figs. 14c,d). The cyclonic circulation error north of Isaac was associated with errors in the upper-level trough over the eastern Gulf of Mexico and the westward extension of the subtropical ridge. The upper-level trough was too strong over the Gulf of Mexico and too weak over the mid-Atlantic coast in the GFS forecast (Figs. 14c,d). The anticyclonic circulation error south of Isaac was associated with errors in the prediction of the

---

[4] Following the methodology of Galarneau and Davis (2013), the steering layer for Isaac at 1200 UTC 26 August was defined as the 850–250-hPa layer using a TC removal radius (r_0) of 2°.
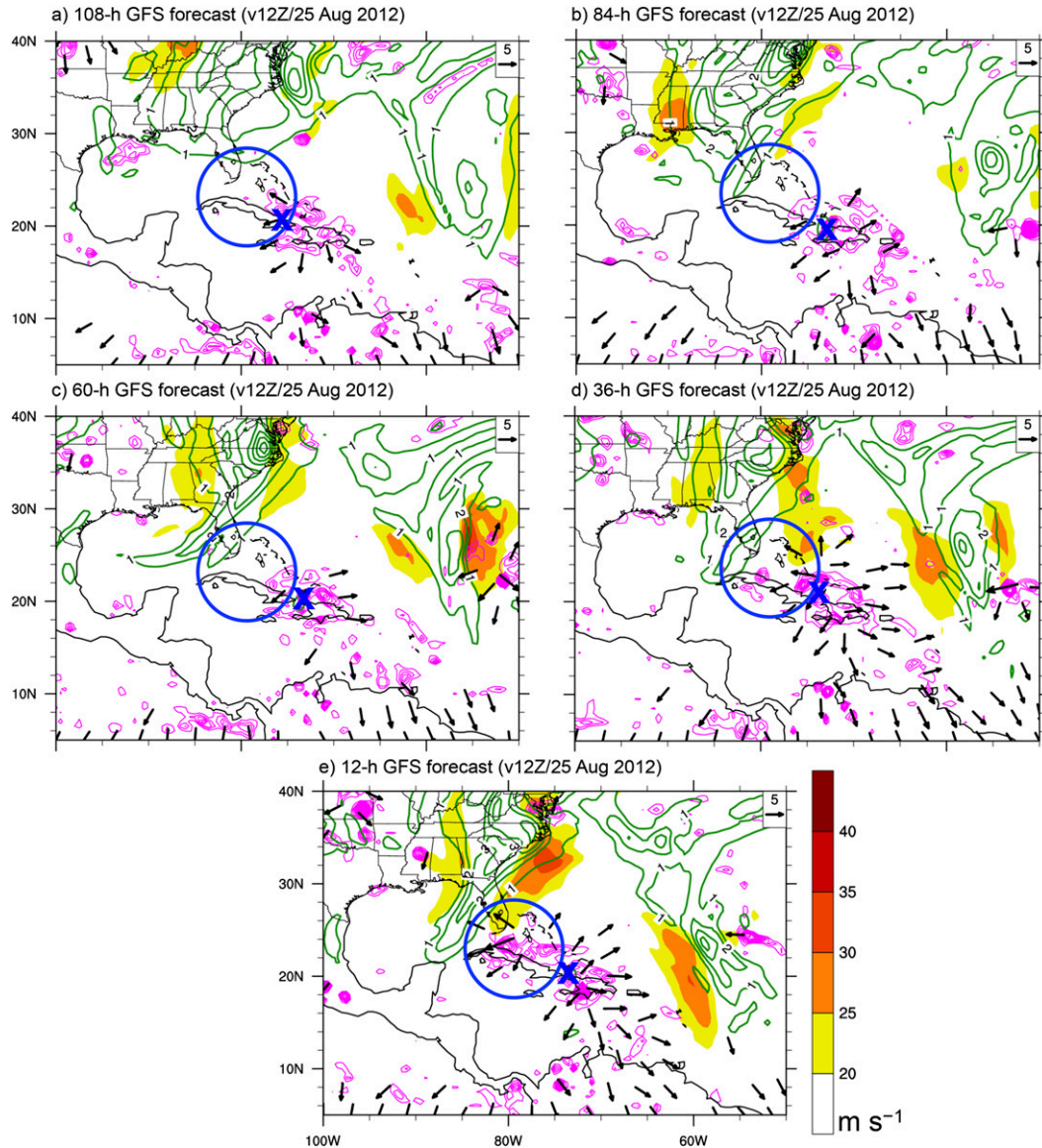
FIG. 13. As in Fig. 8, but for the (a) 108-, (b) 84-, (c) 60-, (d) 36-, and (e) 12-h GFS forecasts verifying at 1200 UTC 25 Aug 2012.

PRE and its attendant low- to midlevel cyclonic vorticity. The PRE was not predicted in the GFS forecast (Figs. 1b and 13b), so its attendant cyclonic vorticity was absent as Isaac approached the Straits of Florida on 26 August (Figs. 14c,d).

The absence of the PRE in the GFS forecast was due, in part, to the lack of a southeasterly tropical moisture feed ahead of Isaac. The evolution of total column PW in the GFS forecast showed the lack of a moisture surge northwest of Isaac on 24 August (Fig. 15a). Total column PW values along the north side of Cuba exceeded 56 mm at 1200 UTC 24 August in the GFS analysis, compared to 44–48 mm in the 60-h GFS forecast

(Figs. 3b and 15b). The disparity increased at 0000 UTC 25 August, with the GFS analysis showing PW values over 60 mm near the developing PRE, compared to 40– 44 mm in the 72-h GFS forecast (Figs. 3c and 15c). In addition to drier conditions in the PRE region northwest of Isaac, the mid- and upper-level deformation zone and frontogenesis was weaker and displaced northeast in the forecast compared to the analysis (Figs. 7a and 16a). The vertical cross section extending from Isaac northwestward into the eastern Gulf of Mexico further illustrated how the 850–400-hPa layer was drier and frontogenesis was weaker in the GFS forecast compared to the analysis northwest of Isaac (Figs. 7b and 16b). The low- to midlevel

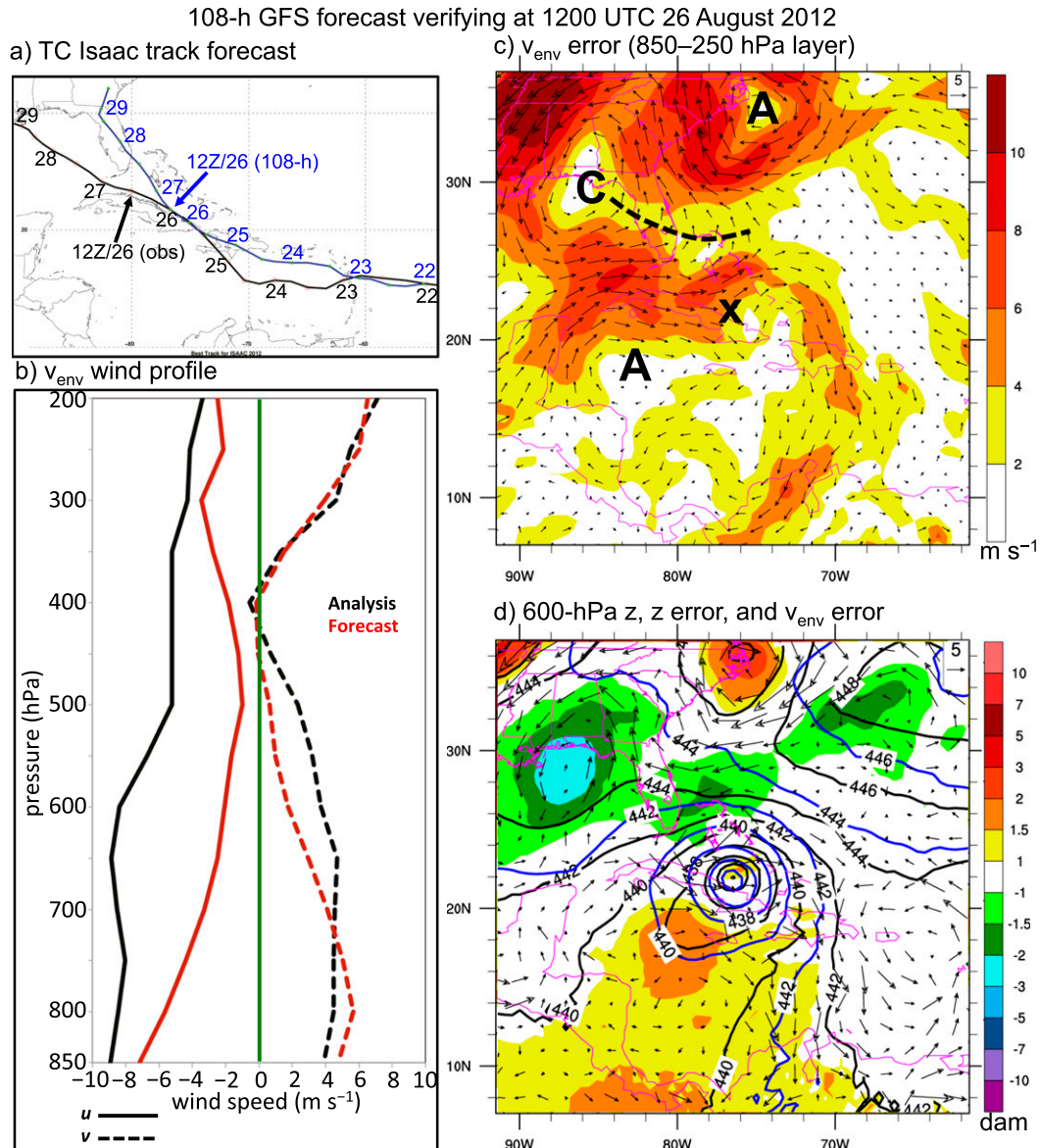108-h GFS forecast verifying at 1200 UTC 26 August 2012

FIG. 14. (a) HURDAT (black line) and GFS (blue) track forecast initialized at 0000 UTC 22 Aug 2012 for TC Isaac. The 0000 UTC positions are marked by circles and the 1200 UTC 26 Aug positions are marked by arrows. (b) TC Isaac $\mathbf{V}_{env}$ (m s^{-1}; defined using $r_0 = 2°$) profile from the GFS analysis (black lines) and 108-h GFS forecast (red lines) verifying at 1200 UTC 26 Aug 2012. The u component is plotted using solid lines and the v component is plotted using dashed lines. The zero contour is marked by the vertical green line. (c) GFS 108-h forecast $\mathbf{V}_{env}$ error (forecast − analysis; arrows with magnitude shaded according to the color bar in m s^{-1} and the scale in top left) vertically averaged in the 850–250-hPa steering layer verifying at 1200 UTC 26 Aug 2012. The anticyclonic circulation errors are marked with an A, the cyclonic circulation error is marked with a C with a dashed line indicating a trough axis, and TC Isaac is marked with an X. (d) GFS 108-h forecast 600-hPa geopotential height (solid contours every 2 dam; analysis in black; forecast in blue), height error (forecast − analysis; shaded according to the color bar in dam), and $\mathbf{V}_{env}$ error (forecast − analysis; arrows in m s^{-1}, and the scale in top left) verifying at 1200 UTC 26 Aug 2012. The grids were shifted so the forecast and observed TC was located in the same position in (c) and (d), so the geography is shown for scale only.

PV anomaly (P) was also absent (Fig. 16c). In all, the ingredients for heavy rainfall—tropical moisture and a lifting mechanism—did not materialize in the GFS forecast. The lack of a tropical moisture surge ahead of Isaac in the GFS forecast appeared to be related to the strength of the southeasterly flow over and northwest of Isaac.

The evolution of 700–500-hPa layer-mean ψ in the GFS forecast and the verifying analysis for 0000 UTC
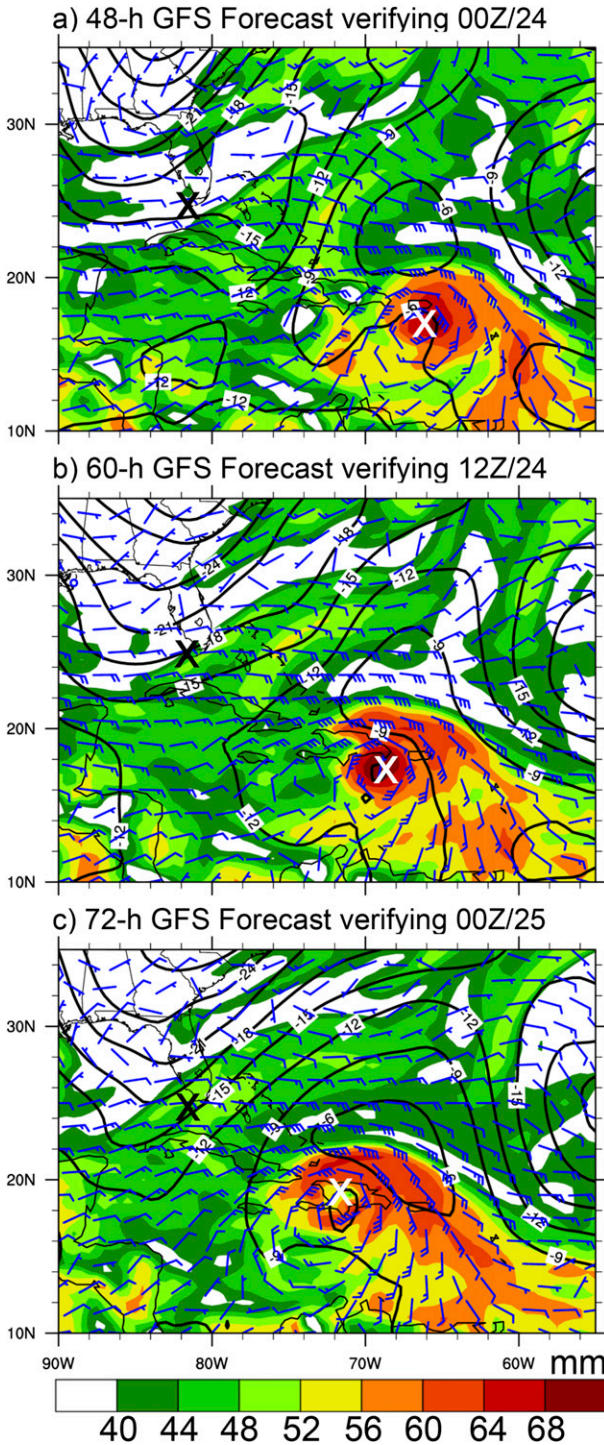
FIG. 15. As in Fig. 3, but for the (a) 48-, (b) 60-, and (c) 72-h GFS forecasts initialized at 0000 UTC 22 Aug 2012.

24 August–1200 UTC 25 August is shown in Fig. 17. In the 48- and 60-h GFS forecast, a cyclonic flow error rapidly developed in the region of the subtropical ridge over the western North Atlantic, while an anticyclonic

flow error developed over the northern Caribbean Sea from Hispaniola to Cuba (Figs. 17a,b). These forecast errors were indicative of a subtropical ridge that was too weak north of Isaac, and a lack of cyclonic vorticity over the northern Caribbean. The strength and structure of the subtropical ridge at 1200 UTC 24 August was linked to upstream extratropical cyclone development over the southeast U.S. coast, with the 60-h GFS forecast predicting weaker cyclone development compared to the verifying analysis (Figs. 18a,b). The 700–500-hPa ψ errors in the GFS forecast increased at 0000 and 1200 UTC 25 August, with the weaker subtropical ridge and lack of PRE cyclonic vorticity resulting in weaker and backed easterly flow compared to strong southeasterly flow northwest of Isaac in the GFS analysis (Figs. 17c,d). By 1200 UTC 25 August, the cyclonic circulation associated with the PRE intensified in the GFS analysis, but was absent in the 84-h GFS forecast (Figs. 17d and 18c,d).

The lack of a northwestward moisture surge ahead of Isaac was linked to a weaker subtropical ridge over the western North Atlantic and a lack of cyclonic vorticity development over the northern Caribbean. The weaker subtropical ridge was linked to weaker upstream extratropical cyclone development over the southeast U.S. coast in the GFS forecast. The reduced meridional gradient of relative vorticity north of Cuba led to flow northwest of Isaac that was weaker and backed to more easterly flow compared to the analysis. The GFS forecast synoptic-scale flow errors interrupted PRE development and attendant cyclonic vorticity amplification over the Straits of Florida, which eliminated the binary interaction (Figs. 18e,f) and easterly steering layer flow (Figs. 14b,c) that acted to move Isaac into the Gulf of Mexico, resulting in Isaac's early recurvature and landfall over Florida.

5. Conclusions

The aim of this study was to examine the PRE that occurred over the Straits of Florida ahead of North Atlantic TC Isaac on 25 August 2012. The PRE produced over 100 mm of rainfall between Cuba and Florida, with widespread flooding documented over southern Florida (Berg 2013). Several studies in the literature have documented the synoptic-scale conditions in which PREs developed ahead of TCs. PREs developed as a plume of tropical moisture moved ahead of the TC in conjunction with a low-level jet and was forced to ascend along a baroclinic zone in the equatorward entrance region of an upper-level jet streak (e.g., Galarneau et al. 2010; Bosart et al. 2012; Moore et al. 2013; Baek et al. 2013). The PRE ahead of TC Isaac documented in this paper was unique compared to previously documented PREs in that it occurred in the oceanic subtropical latitudes and the bulk-upscale effect of
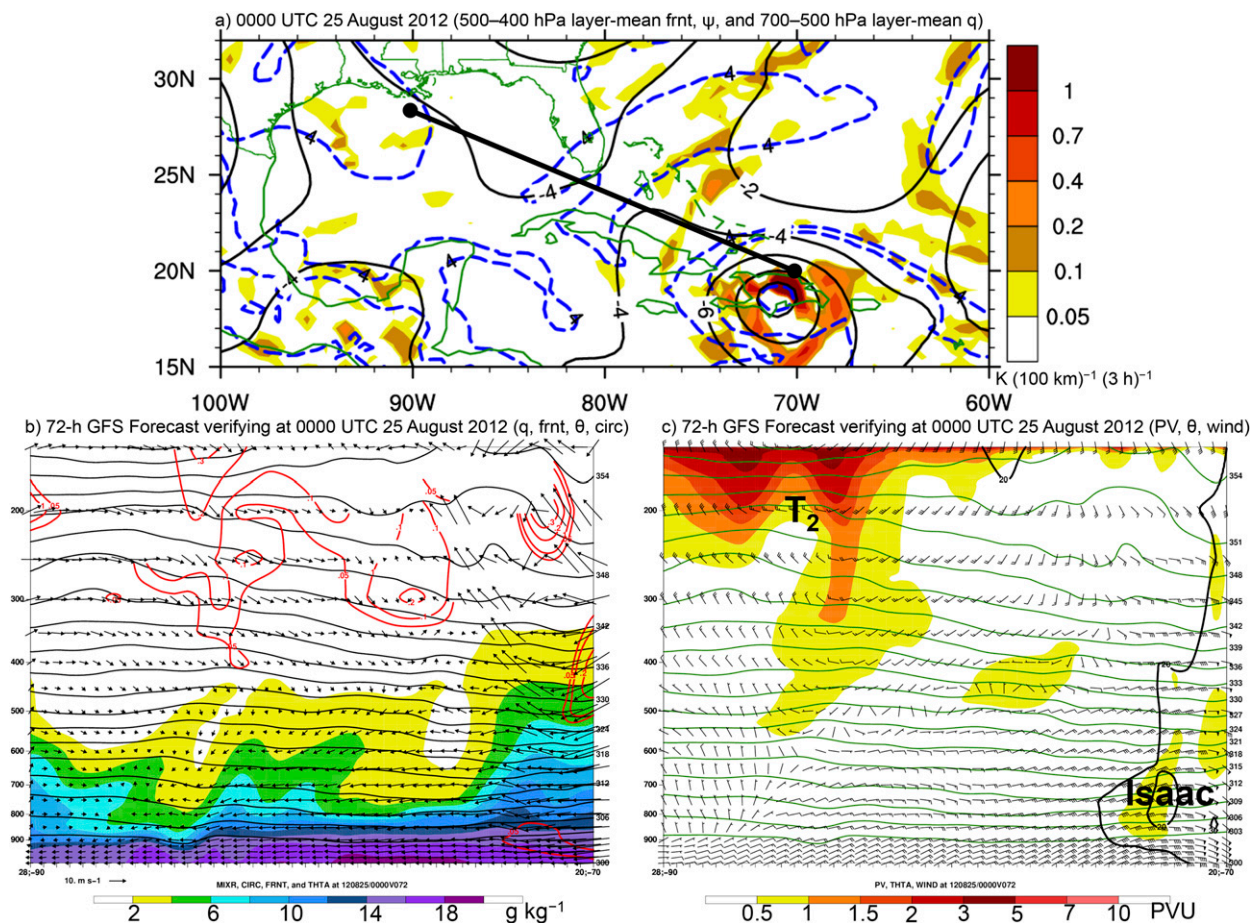
FIG. 16. (a)–(c) As in Figs. 7a–c, but for the 72-h GFS forecast verifying at 0000 UTC 25 Aug 2012.

its deep convection altered the synoptic-scale environment and steering flow of an approaching TC. The PRE helped to steer TC Isaac through the Straits of Florida into the eastern Gulf of Mexico on 25–26 August, rather than recurve Isaac over Florida. The inability of the 0000 UTC operational GFS forecasts initialized prior to 25 August to accurately represent the PRE, and as a result recurve Isaac over Florida and the extreme eastern Gulf of Mexico, highlighted the difficult forecast challenge in anticipating how the complex interaction between a PRE and its surrounding environment will impact a TC approaching the U.S. mainland.

Comparison of the synoptic-scale flow pattern of the PRE with the classification by Moore et al. (2013) showed that the Isaac PRE most resembled the southwesterly jet (SJ) classification, except that the TC did not *directly* impact the upper-level jet and influence the maintenance of the PRE. The TC played an *indirect* role in PRE formation and maintenance by supplying tropical moisture only, much like PREs in the jet in ridge (JR) category, despite a synoptic pattern that resembled the SJ category. The

character of the tropical moisture feed and lifting mechanisms that organized the PRE also differed from PREs documented in the midlatitudes. The tropical moisture feed for the PRE ahead of Isaac was characterized by total column PW values over 60 mm (Figs. 3b–d), compared to more typical values of 50 mm for the midlatitude SJ PREs documented in Moore et al. (2013, see their Fig. 9f). The lifting mechanism for the PRE ahead of Isaac also differed from midlatitude SJ PREs, with weaker frontogenesis and warm advection in the mid- and upper troposphere and an absence of a coherent lifting mechanism in the lower troposphere during PRE initiation [cf. our Fig. 7b with Moore et al.'s (2013) Fig. 11].

The differences in moisture and synoptic-scale lift between the Isaac PRE and typical midlatitude PREs suggests that PREs over the oceanic subtropics may occur in environments with more abundant tropical moisture as would be expected of a maritime tropical air mass over a warm ocean. A systematic climatology of oceanic subtropical PREs is needed to establish the significant environmental differences between oceanic subtropical PREs
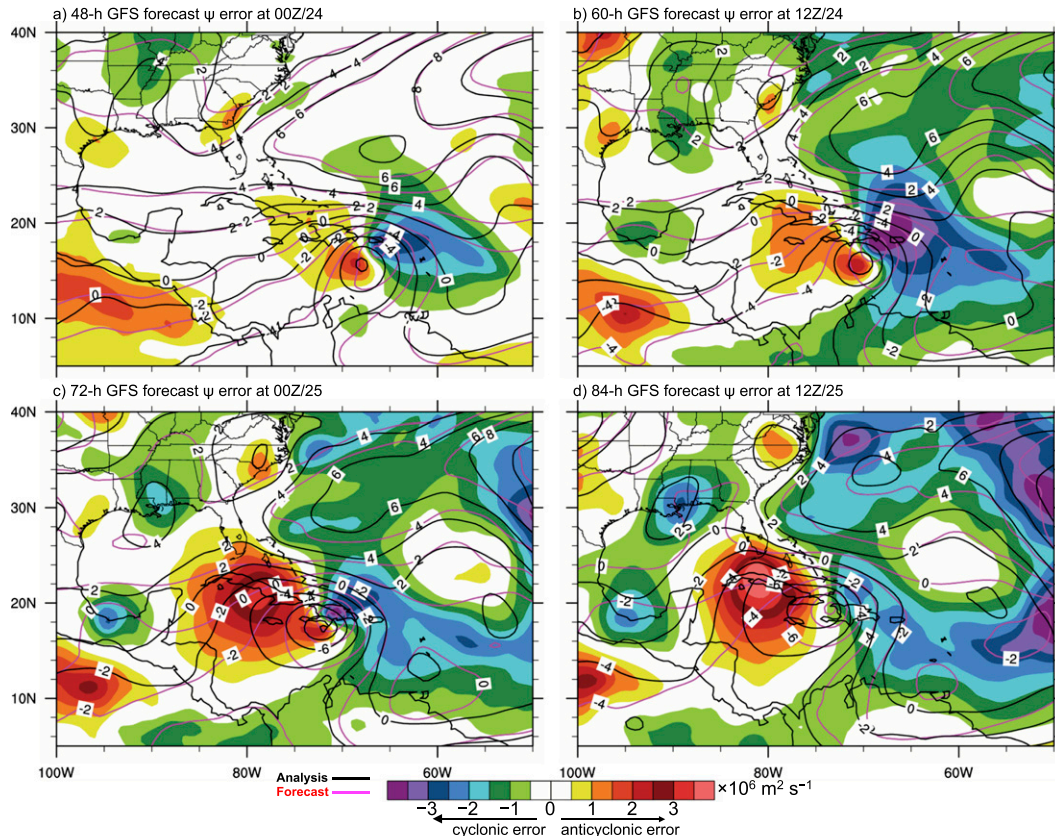
FIG. 17. The 700–500-hPa layer-mean ψ (solid contours every $2.0 \times 10^6 \, \mathrm{m}^2 \, \mathrm{s}^{-1}$; GFS analysis in black; GFS forecast in magenta) and GFS forecast ψ error (forecast − analysis; shaded according to the color bar in $\times 10^6 \, \mathrm{m}^2 \, \mathrm{s}^{-1}$) for the (a) 48-, (b) 60-, (c) 72-, and (d) 84-h GFS forecast initialized at 0000 UTC 22 Aug 2012.

and midlatitude PREs. Implications for the increased moisture and attendant reduced static stability for subtropical PREs compared to midlatitude PREs are that weaker lifting mechanisms are needed to aid in the development of heavy rainfall and that the precipitation efficiency is increased in the oceanic maritime tropical air mass (e.g., Market et al. 2003; Gochis et al. 2015).

Another unique aspect of the PRE ahead of TC Isaac was its impact on the synoptic-scale environment flow, which influenced the track of TC Isaac on 25–27 August while it threatened south Florida. Convectively driven divergent outflow associated with the PRE contributed to thinning and fracture of the upper-level trough over Florida and the eastern Gulf of Mexico. The influence of upper-level diabatically driven divergent outflow on PV gradients has been well documented (e.g., Archambault et al. 2013, 2015). From a more general perspective, upper-level troughs (or PV streamers) are driven into subtropical latitudes on the forward flank of anticyclonic Rossby wave breaking (AWB) events (Martius et al. 2008). These PV streamers are stretched into long filaments by increased deformation on the periphery of the

upstream anticyclone, and eventually fracture into cutoff circulations (Wernli and Sprenger 2007). The fracture of PV streamers can also be aided by convectively driven divergent outflow from heavy-rain-producing convective systems (e.g., Morgenstern and Davies 1999) bearing similarity to the Isaac PRE, or developing TCs (e.g., Galarneau et al. 2015) on the southeast flank of the PV streamer.

Forecast errors in the structure and evolution of synoptic-scale weather systems and their role in TC track forecast errors are well documented (e.g., Carr and Elsberry 2000; Majumdar et al. 2006; Wu et al. 2009; Brennan and Majumdar 2011). Recent studies of track forecasts for TC Sandy (2012) have also clearly shown that deep convection in close proximity to the TC can influence the synoptic-scale flow near the TC resulting in large track errors (e.g., Torn et al. 2015; Bassill 2014, 2015; Munsell and Zhang 2014). Errors in convection on the periphery of TC Sandy have been linked to initial condition errors (Torn et al. 2015) and treatment of convection by cumulus parameterizations (Bassill 2014, 2015). In the case of TCs Sandy and Isaac, errors in the prediction of upper-level divergent outflow either by
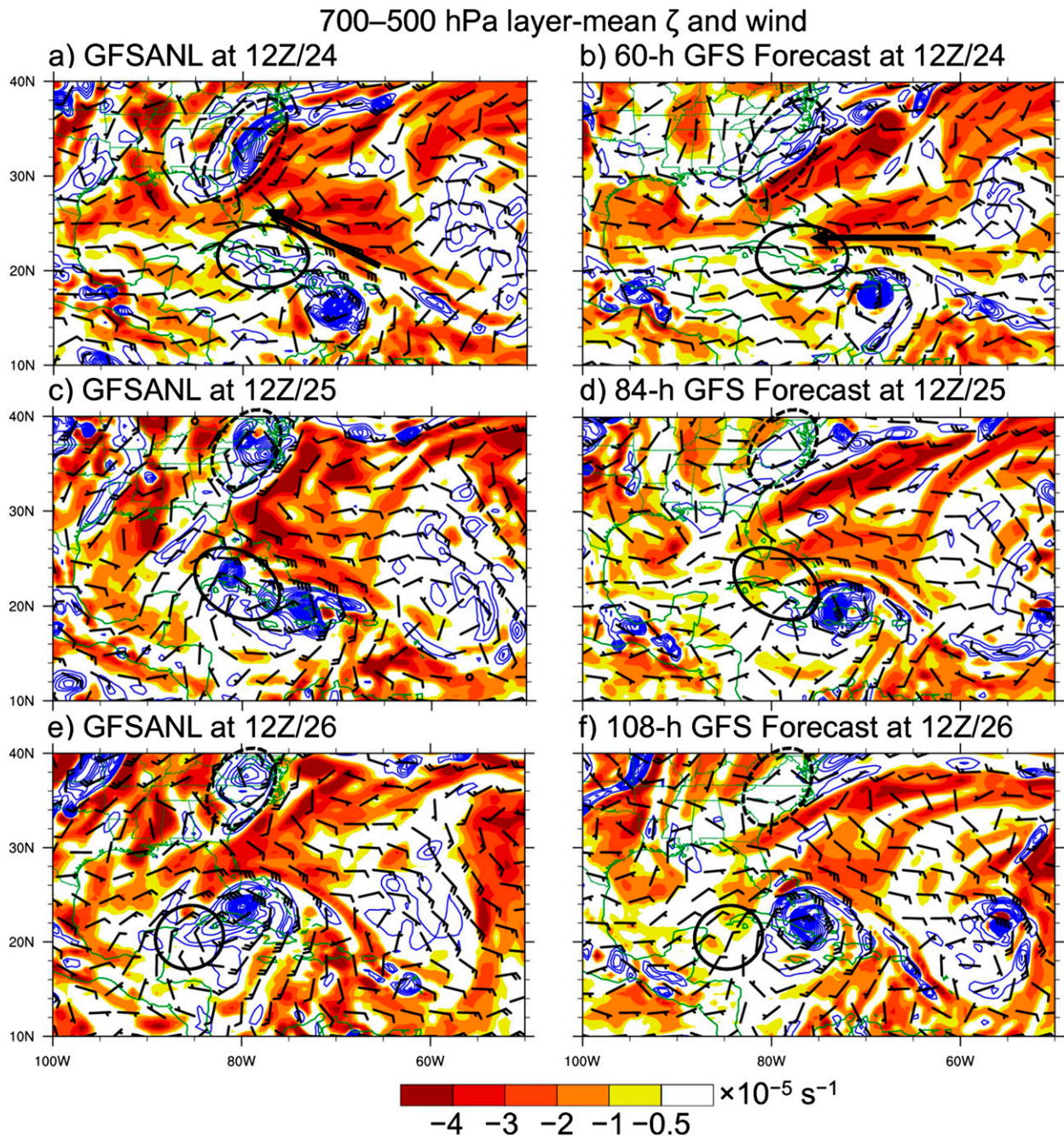
700–500 hPa layer-mean ζ and wind

FIG. 18. The 700–500-hPa layer-mean relative vorticity (anticyclonic shaded according to the color bar in $\times 10^{-5}\,\mathrm{s}^{-1}$; cyclonic contoured every $2.0 \times 10^{-5}\,\mathrm{s}^{-1}$ starting at $2.0 \times 10^{-5}\,\mathrm{s}^{-1}$) and wind vector (barbs as in Fig. 3) from the (a) GFS analysis and (b) 60-h GFS forecast verifying at 1200 UTC 24 Aug, (c) GFS analysis and (d) 84-h GFS forecast verifying at 1200 UTC 25 Aug, and (e) GFS analysis and (f) 108-h GFS forecast verifying at 1200 UTC 26 Aug 2012. The PRE vorticity (P) and coastal extratropical cyclone (C) are marked by the solid and dashed black ellipses, respectively. The flow north of Isaac at 1200 UTC 24 Aug 2012 is marked by the black arrow.

convection on the periphery of a TC (Torn et al. 2015) or associated with a nearby PRE, and its impact on pre-existing upper-level circulation features and generation/amplification of low- to midlevel circulation features, can have a large impact on the TC track. The impact of improved

representation of atmospheric water vapor in the near-TC environment by assimilating observations from the Continuously Operating Caribbean Global Positioning System Observational Network (COCONet; Braun et al. 2012) on numerical forecasts of convection on the

periphery of TCs Isaac and Sandy may be a useful future research initiative.

Systematic examination of the predictability and forecastability of PREs in the midlatitudes and subtropics in operational numerical weather prediction models is a logical next step in research on PREs that may have direct applicability to operations. Given the relative rarity of TCs and PREs compared to, for example, the occurrence of drizzle, the use of a long time series of ensemble forecasts (termed "reforecasts") as recently developed by NOAA (Hamill et al. 2013) may prove fruitful.

REFERENCES

Archambault, H. M., L. F. Bosart, D. Keyser, and J. M. Cordeira, 2013: A climatological analysis of the extratropical flow response to recurving western North Pacific tropical cyclones. *Mon. Wea. Rev.,* **141,** 2325–2346, doi:10.1175/MWR-D-12-00257.1.

——, D. Keyser, L. F. Bosart, C. A. Davis, and J. M. Cordeira, 2015: A composite perspective of the extratropical flow response to recurving western North Pacific tropical cyclones. *Mon. Wea. Rev.,* **143,** 1122–1141, doi:10.1175/MWR-D-14-00270.1.

Baek, E.-H., J.-H. Kim, J.-S. Kug, and G.-H. Lim, 2013: Favorable versus unfavorable synoptic backgrounds for indirect precipitation events ahead of tropical cyclones approaching the Korean Peninsula: A comparison of two cases. *Asia-Pac. J. Atmos. Sci.,* **49,** 333–346, doi:10.1007/s13143-013-0032-z.

Bassill, N. P., 2014: Accuracy of early GFS and ECMWF Sandy (2012) track forecasts: Evidence for a dependence on cumulus parameterization. *Geophys. Res. Lett.,* **41,** 3274–3281, doi:10.1002/2014GL059839.

——, 2015: An analysis of the operational GFS Simplified Arakawa Schubert parameterization within a WRF framework: A Hurricane

Sandy (2012) long-term track perspective. *J. Geophys. Res. Atmos.,* **120,** 378–398, doi:10.1002/2014JD022211.

Berg, R., 2013: Tropical cyclone report: Hurricane Isaac. Tech. Rep. AL092012, NOAA/National Hurricane Center, 78 pp. [Available online at http://www.nhc.noaa.gov/data/tcr/AL092012_Isaac.pdf.]

Bosart, L. F., and F. H. Carr, 1978: A case study of excessive rainfall centered around Wellsville, New York, 20–21 June 1972. *Mon. Wea. Rev.,* **106,** 348–362, doi:10.1175/1520-0493(1978)106<0348:ACSOER>2.0.CO;2.

——, J. M. Cordeira, T. J. Galarneau Jr., B. J. Moore, and H. M. Archambault, 2012: An analysis of multiple predecessor rain events ahead of Tropical Cyclones Ike and Lowell: 10–15 September 2008. *Mon. Wea. Rev.,* **140,** 1081–1107, doi:10.1175/MWR-D-11-00163.1.

Braun, J. J., and Coauthors, 2012: Focused study of interweaving hazards across the Caribbean. *Eos, Trans. Amer. Geophys. Union,* **93,** 89–90, doi:10.1029/2012EO090001.

Brennan, M. J., and S. J. Majumdar, 2011: An examination of model track forecast errors for Hurricane Ike (2008) in the Gulf of Mexico. *Wea. Forecasting,* **26,** 848–867, doi:10.1175/WAF-D-10-05053.1.

Byun, K.-Y., and T.-Y. Lee, 2012: Remote effects of tropical cyclones on heavy rainfall over the Korean peninsula—Statistical and composite analysis. *Tellus,* **64A,** 14983, doi:10.3402/tellusa.v64i0.14983.

Carr, L. E., and R. L. Elsberry, 2000: Dynamical tropical cyclone track forecast errors. Part I: Tropical region error sources. *Wea. Forecasting,* **15,** 641–661, doi:10.1175/1520-0434(2000)015<0641:DTCTFE>2.0.CO;2.

Cordeira, J. M., F. M. Ralph, and B. J. Moore, 2013: The development and evolution of two atmospheric rivers in proximity to western North Pacific tropical cyclones in October 2010. *Mon. Wea. Rev.,* **141,** 4234–4255, doi:10.1175/MWR-D-13-00019.1.

Cote, M. R., 2007: Predecessor rain events in advance of tropical cyclones. M.S. thesis, Department of Earth and Atmospheric Sciences, University at Albany, State University of New York, 200 pp. [Available online at http://cstar.cestm.albany.edu/CAP_Projects/Project10/index.htm.]

Davis, C., C. Snyder, and A. C. Didlake Jr., 2008: A vortex-based perspective of eastern Pacific tropical cyclone formation. *Mon. Wea. Rev.,* **136,** 2461–2477, doi:10.1175/2007MWR2317.1.

Dong, K., and C. J. Neumann, 1983: On the relative motion of binary tropical cyclones. *Mon. Wea. Rev.,* **111,** 945–953, doi:10.1175/1520-0493(1983)111<0945:OTRMOB>2.0.CO;2.

Doswell, C. A., III, H. E. Brooks, and R. A. Maddox, 1996: Flash flood forecasting: An ingredients-based methodology. *Wea. Forecasting,* **11,** 560–581, doi:10.1175/1520-0434(1996)011<0560:FFFAIB>2.0.CO;2.

Fujiwhara, S., 1923: On the growth and decay of vortical systems. *Quart. J. Roy. Meteor. Soc.,* **49,** 75–104, doi:10.1002/qj.49704920602.

——, 1931: Short note on the behavior of two vortices. *Proc. Phys.—Math. Soc. Japan, Ser. 3,* **13,** 106–110.

Galarneau, T. J., Jr., and C. A. Davis, 2013: Diagnosing forecast errors in tropical cyclone motion. *Mon. Wea. Rev.,* **141,** 405–430, doi:10.1175/MWR-D-12-00071.1.

——, L. F. Bosart, and R. S. Schumacher, 2010: Predecessor rain events ahead of tropical cyclones. *Mon. Wea. Rev.,* **138,** 3272–3297, doi:10.1175/2010MWR3243.1.

——, R. McTaggart-Cowan, L. F. Bosart, and C. A. Davis, 2015: Development of North Atlantic tropical disturbances near upper-level potential vorticity streamers. *J. Atmos. Sci.,* **72,** 572–597, doi:10.1175/JAS-D-14-0106.1.

Gall, R., F. Toepfer, F. Marks, and E. Rappaport, 2014: Hurricane Forecast Improvement Project Years Five to Ten Strategic Plan. HFIP Tech. Rep. HFIP2014-1.1a, NOAA/Hurricane Forecast Improvement Project, 44 pp. [Available online at http://www.hfip.org/documents/HFIP_StrategicPlan_Yrs5-10_Nov05_2014_Update.pdf.]

Gochis, D., and Coauthors, 2015: The Great Colorado Flood of September 2013. *Bull. Amer. Meteor. Soc.,* doi:10.1175/BAMS-D-13-00241.1, in press.

Hamill, T. M., G. T. Bates, J. S. Whitaker, D. R. Murray, M. Fiorino, T. J. Galarneau Jr., Y. Zhu, and W. Lapenta, 2013: NOAA's second-generation global medium-range ensemble reforecast dataset. *Bull. Amer. Meteor. Soc.,* **94,** 1553–1565, doi:10.1175/BAMS-D-12-00014.1.

Joyce, R. J., J. E. Janowiak, P. A. Arkin, and P. Xie, 2004: CMORPH: A method that produces global precipitation estimates from passive microwave and infrared data at high spatial and temporal resolution. *J. Hydrometeor.,* **5,** 487–503, doi:10.1175/1525-7541(2004)005<0487:CAMTPG>2.0.CO;2.

Keyser, D., M. J. Pecnick, and M. A. Shapiro, 1986: Diagnosis of the role of vertical deformation in a two-dimensional primitive equation model of upper-level frontogenesis. *J. Atmos. Sci.,* **43,** 839–850, doi:10.1175/1520-0469(1986)043<0839:DOTROV>2.0.CO;2.

Landsea, C., and Coauthors, 2004: The Atlantic hurricane database reanalysis project: Documentation for the 1851–1910 alterations and additions to the HURDAT database. *Hurricanes and Typhoons: Past, Present, and Future,* R. J. Murname and K.-B. Liu, Eds., Columbia University Press, 177–221.

Maddox, R. A., C. F. Chappell, and L. R. Hoxit, 1979: Synoptic and meso-α scale aspects of flash flood events. *Bull. Amer. Meteor. Soc.,* **60,** 115–123, doi:10.1175/1520-0477-60.2.115.

Majumdar, S. J., S. D. Aberson, C. H. Bishop, R. Buizza, M. S. Peng, and C. A. Reynolds, 2006: A comparison of adaptive observing guidance for Atlantic tropical cyclones. *Mon. Wea. Rev.,* **134,** 2354–2372, doi:10.1175/MWR3193.1.

Market, P., S. Allen, R. Scofield, R. Kuligowski, and A. Gruber, 2003: Precipitation efficiency of warm-season Midwestern mesoscale convective systems. *Wea. Forecasting,* **18,** 1273–1285, doi:10.1175/1520-0434(2003)018<1273:PEOWMM>2.0.CO;2.

Martius, O., C. Schwierz, and M. Sprenger, 2008: Dynamical tropopause variability and potential vorticity streamers in the Northern Hemisphere—A climatological analysis. *Adv. Atmos. Sci.,* **25,** 367–380, doi:10.1007/s00376-008-0367-z.

Meng, Z., and Y. Zhang, 2012: On the squall lines preceding landfalling tropical cyclones in China. *Mon. Wea. Rev.,* **140,** 445–470, doi:10.1175/MWR-D-10-05080.1.

Minnesota Department of Natural Resources, 2015: Heavy rains fall on southeastern Minnesota: August 18–20, 2007. Accessed 14 January 2015. [Available online at http://www.dnr.state.mn.us/climate/journal/ff070820.html.]

Moore, B. J., P. J. Neiman, F. M. Ralph, and F. E. Barthold, 2012: Physical processes associated with heavy flooding rainfall in Nashville, Tennessee, and vicinity during 1–2 May 2010: The role of an atmospheric river and mesoscale convective systems. *Mon. Wea. Rev.,* **140,** 358–378, doi:10.1175/MWR-D-11-00126.1.

——, L. F. Bosart, D. Keyser, and M. L. Jurewicz, 2013: Synoptic-scale environments of predecessor rain events occurring east of the Rocky Mountains in association with Atlantic basin tropical cyclones. *Mon. Wea. Rev.,* **141,** 1022–1047, doi:10.1175/MWR-D-12-00178.1.

Morgenstern, O., and H. C. Davies, 1999: Disruption of an upper-level PV-streamer by orographic and cloud-diabatic effects. *Contrib. Atmos. Phys.,* **72,** 173–186.

Munsell, E. B., and F. Zhang, 2014: Prediction and uncertainty of Hurricane Sandy (2012) explored through a real-time cloud-permitting ensemble analysis and forecast system assimilating airborne Doppler radar observations. *J. Adv. Model. Earth Syst.,* **6,** 38–58, doi:10.1002/2013MS000297.

Riemer, M., and S. C. Jones, 2014: Interaction of a tropical cyclone with a high-amplitude, midlatitude wave pattern: Waviness analysis, trough deformation and track bifurcation. *Quart. J. Roy. Meteor. Soc.,* **140,** 1362–1376, doi:10.1002/qj.2221.

Rowe, S. T., and G. Villarini, 2013: Flooding associated with predecessor rain events over the Midwest United States. *Environ. Res. Lett.,* **8,** 024007, doi:10.1088/1748-9326/8/2/024007.

Rozoff, C. M., W. H. Schubert, B. D. McNoldy, and J. P. Kossin, 2006: Rapid filamentation zones in intense tropical cyclones. *J. Atmos. Sci.,* **63,** 325–340, doi:10.1175/JAS3595.1.

Schumacher, R. S., and T. J. Galarneau Jr., 2012: Moisture transport into midlatitudes ahead of recurving tropical cyclones and its relevance in two predecessor rain events. *Mon. Wea. Rev.,* **140,** 1810–1827, doi:10.1175/MWR-D-11-00307.1.

——, ——, and L. F. Bosart, 2011: Distant effects of a recurving tropical cyclone on rainfall in a midlatitude convective system: A high-impact predecessor rain event. *Mon. Wea. Rev.,* **139,** 650–667, doi:10.1175/2010MWR3453.1.

Simpson, R. H., 1974: The hurricane disaster potential scale. *Weatherwise,* **27,** 169–186, doi:10.1080/00431672.1974.9931702.

Torn, R. D., J. S. Whitaker, P. Pegion, T. M. Hamill, and G. J. Hakim, 2015: Diagnosis of the source of GFS medium-range track errors in Hurricane Sandy (2012). *Mon. Wea. Rev.,* **143,** 132–152, doi:10.1175/MWR-D-14-00086.1.

Wang, Y., Y. Wang, and H. Fudeyasu, 2009: The role of Typhoon Songda (2004) in producing distantly located heavy rainfall in Japan. *Mon. Wea. Rev.,* **137,** 3699–3716, doi:10.1175/2009MWR2933.1.

Wernli, H., and M. Sprenger, 2007: Identification and ERA-15 climatology of potential vorticity streamers and cutoffs near the extratropical tropopause. *J. Atmos. Sci.,* **64,** 1569–1586, doi:10.1175/JAS3912.1.

Wu, C. C., and Coauthors, 2009: Intercomparison of targeted observation guidance for tropical cyclones in the northwestern Pacific. *Mon. Wea. Rev.,* **137,** 2471–2492, doi:10.1175/2009MWR2762.1.